New MRI-based methods for the identification of cortical and subcortical eloquent brain areas
Implementations in pediatric patients

PhD Thesis

Adrienn Máté, MD

Clinical and Experimental Neuroscience Program
Doctoral School of Clinical Medicine
Faculty of Medicine
University of Szeged

Supervisor: Pál Barzó, MD, DSc
Department of Neurosurgery
Faculty of Medicine
University of Szeged

Szeged
2019

Table of Contents

Original publications directly related to the thesis:

I. Máté A, Lidzba K, Hauser TK, Staudt M, Wilke M: A "one size fits all" approach to language fMRI: increasing specificity and applicability by adding a self-paced component. Exp Brain Res. 2016 Mar;234(3):673-84.

IF: 1,89

II. Máté A, Kis D, Czigner A, Fischer T, Halász L, Barzó P: Connectivity-based segmentation of the brainstem by probabilistic tractography. Brain Res. 2018 Jul 1;1690:74-88.

IF: 3,125

Original publications not directly related to the thesis:

III. Zombor M, Kalmár T, Maróti Z, Zimmermann A, **Máté A**, Bereczki C, Sztriha L: Co-occurrence of mutations in FOXP1 and PTCH1 in a girl with extreme megalencephaly, callosal dysgenesis and profound intellectual disability. J Hum Genet. 2018 Nov;63(11):1189-1193.

IF: 3,545

IV. Carter J, Zombor M, **Máté A**, Sztriha L, Waters JJ: De Novo Interstitial Microdeletion at 1q32.1 in a 10-Year-Old Boy with Developmental Delay and Dysmorphism. Case Rep Genet. 2016;2016:2501741. doi: 10.1155/2016/2501741.

IF: 0

V. Zádori D, **Máté A**, Róna-Vörös K, Gergev G, Zimmermann A, Nagy N, Széll M, Vécsei L, Sztriha L, Klivényi P: The clinical manifestations of two novel SPAST mutations. Clin Neurol Neurosurg. 2015 Sep;136:82-85.

IF: 1,198

VI. Thiffault I, Wolf NI, Forget D, Guerrero K, Tran LT, Choquet K, Lavallée-Adam M, Poitras C, Brais B, Yoon G, Sztriha L, Webster RI, Timmann D, van de Warrenburg BP, Seeger J, Zimmermann A, **Máté A**, Goizet C, Fung E, van der Knaap MS, Fribourg S, Vanderver A, Simons C, Taft RJ, Yates JR 3rd, Coulombe B, Bernard G: Recessive mutations in POLR1C cause a leukodystrophy by impairing biogenesis of RNA polymerase III. Nat Commun. 2015 Jul 7;6:7623.

IF: 11,329

VII. Gergev G, **Máté A**, Zimmermann A, Rárosi F, Sztriha L: Spectrum of neurodevelopmental disabilities: a cohort study in Hungary. J Child Neurol. 2015 Mar;30(3):344-56.

IF: 1,434

VIII. Kis D, **Máté A**, Kincses ZT, Vörös E, Barzó P: The role of probabilistic tractography in the surgical treatment of thalamic gliomas. Neurosurgery. 2014 Jun;10 Suppl 2:262-272; discussion 272.

IF: 3,62

IX. Romani M, Micalizzi A, Kraoua I, Dotti MT, Cavallin M, Sztriha L, Ruta R, Mancini F, Mazza T, Castellana S, Hanene B, Carluccio MA, Darra F, **Máté A**, Zimmermann A, Gouider-Khouja N, Valente EM: Mutations in B9D1 and MKS1 cause mild Joubert syndrome: expanding the genetic overlap with the lethal ciliopathy Meckel syndrome. Orphanet J Rare Dis. 2014 May 5;9:72. doi: 10.1186/1750-1172-9-72.

IF: 3,358

X. Eggens VR, Barth PG, Niermeijer JM, Berg JN, Darin N, Dixit A, Fluss J, Foulds N, Fowler D, Hortobágyi T, Jacques T, King MD, Makrythanasis P, **Máté A**, Nicoll JA, O'Rourke D, Price S, Williams AN, Wilson L, Suri M, Sztriha L, Dijns-de Wissel MB, van Meegen MT, van Ruissen F, Aronica E, Troost D, Majoie CB, Marquering HA, Poll-Thé BT, Baas F: EXOSC3 mutations in pontocerebellar hypoplasia type 1: novel mutations and genotype-phenotype correlations. Orphanet J Rare Dis. 2014 Feb 13;9:23. doi: 10.1186/1750-1172-9-23.

IF: 3,358

XI. Monostori P, Baráth A, Fazekas I, Hódi E, **Máté A**, Farkas I, Hracskó Z, Varga IS, Sümegi V, Gellén B, Bereczki C, Túri S: Microvascular reactivity in lean, overweight, and obese hypertensive adolescents. Eur J Pediatr. 2010 Nov;169(11):1369-1374.

IF: 1,644

Scientometry:

Total impact factor: 34,501

Citation index: 140

H-index: 6

Abbreviations

3D IR-FSPGR - 3D inversion recovery-prepared fast spoiled gradient-echo

ALIC - anterior limb of the internal capsule

ARAS - ascending reticular activating system

ASSET - array coil spatial sensitivity encoding

BL - block

BOLD - blood-oxygen level dependent

CDR - connectivity-defined region

CM - connectivity map

CNS - central nervous system

CoG_{conn} - center of gravity of the connectivity values

CST/CBT - corticospinal and corticobulbar tracts

DARTEL - Diffeomorphic Anatomical Registration Through Exponentiated Lie Algebra

DTI - diffusion tensor imaging

DTT - diffusion tensor tractography

EPI - echo planar imaging

ER - event-related

FA - fractional anisotropy

FDR - false discovery rate

FDT - FMRIB's diffusion toolbox

FLAIR - fluid-attenuated inversion recovery

FLIRT - FMRIB's linear image registration tool

fMRI - functional magnetic resonance imaging

FMRIB - Oxford Centre for Functional MRI of the Brain

FOV - field of view

FSL - FMRIB's software library

FWE - family-wise error

IFG - inferior frontal gyrus

ISI - interstimulus interval

LI - lateralization index

MNI152 - Montreal Neurological Institute 152

MRI - magnetic resonance imaging

PDM - probability distribution map

PLIC - posterior limb of the internal capsule

PPVT - Peabody picture vocabulary test

rp - Pearson's coefficient

rs - Spearman's rho

RT - response time

SD - standard deviation

SOA - stimulus onset asynchrony

SYN - synonyms task

SYN_{AC} - active condition of the synonyms task

SYN_{CC} - control condition of the synonyms task

SWI - susceptibility-weighted imaging

TBI - traumatic brain injury

TE - echo time

TI - inversion time

TR - repetition time

VIT - vowel identification task

VIT_{AC} - active condition of the vowel identification task

VIT_{CC} - control condition of the vowel identification task

Magnetic resonance imaging (MRI) is one of the most frequently used imaging modalities of the central nervous system (CNS). Certain types of MRI examinations have the advantage to provide detailed information non-invasively not only from the morphological, but also the functional characteristics of the brain in vivo. The aim of my PhD research was the elaboration of non-invasive MRI-based imaging methods that can serve as potential clinical tools in the diagnosis and therapy of several diseases of the CNS. My work covered two main fields: the methodological improvement of an fMRI language task battery and connectivity-based segmentation of the brainstem by probabilistic tractography. Considering the different methodology and character of these works they are discussed in separate chapters below.

Self-paced paradigm and event-related analysis for increased specificity and applicability of pediatric language functional MRI

Introduction

Basics of functional magnetic resonance imaging

In the past three decades functional magnetic resonance imaging (fMRI) has earned great popularity in neuroimaging mainly due to its non-invasive approach, widespread availability and relatively good spatial resolution. It has brought the possibility to investigate task-induced cognitive state changes or the result of unregulated processes in the resting brain.

Functional MRI uses blood-oxygen level dependent (BOLD) contrast to detect activations and deactivations of a brain region (Ogawa *et al.*, 1990a, b, c; Bandettini *et al.,* 1992; Kwong *et al.,* 1992; Ogawa *et al.,* 1993). When a brain region is activated during a cognitive task, its blood supply is increased within a few seconds (hemodynamic response function). Oxyhemoglobin is diamagnetic, while deoxyhemoglobin is strongly paramagnetic (Thulborn *et al.,* 1982). BOLD contrast can be obtained as the fluctuations in the concentration of deoxygenated hemoglobin create local gradients in the magnetic field surrounding the red blood cells in the capillary beds of an activated brain region. Generally, these differences are very subtle and therefore can be detected by repeated induction of two or more cognitive states (active and control conditions). These cognitive states ideally differ only in the cognitive function in question and the acquired scans are contrasted to find the difference of brain activity between the two (or more) conditions. A very simple example of an fMRI task is finger tapping in the active condition alternated by rest in the control condition. An important characteristic of an fMRI experiment is the design, i.e. how the stimuli of the active and the control condition are arranged during a session. Three main types of design can be distinguished:

In case of block-design stimuli of each condition are arranged in blocks, e.g., in the first 30 seconds of the session stimuli of only the active condition are presented, while in the next 30 seconds only stimuli of the control condition are displayed and so

on. The advantage of this design is its statistical robustness (high detection power, i.e. design efficacy) (Friston *et al.*, 1999), while the effects of habituation and predictability also have to be taken into account.

In case of event-related design (Liu, 2012) active and control stimuli follow each other in a random order and at variable time intervals (interstimulus interval - ISI), which makes this design much less predictable. However, it cannot provide that high design efficacy (Mechelli, Price *et al.,* 2003), albeit it has a higher sensitivity to study the shape and the time course of the hemodynamic response (high estimation power).

Mixed design carries the characteristics of both the block and the event related designs, because stimuli are presented in blocks (active and control) but within the blocks the intervals between the stimuli are varied.

In the past almost 30 years of fMRI history numerous well-established fMRI task batteries have been developed that provide possibility to identify regions responsible for a certain function, e.g., motor activity, speech or spatial orientation.

Increasing applicability and specificity of a widely used pediatric language task battery: modifications of the vowel identification and the synonyms tasks

Noninvasive language mapping by fMRI is increasingly used to identify the language-dominant hemisphere in the context of presurgical evaluation (Benson *et al.,* 1999; Lehericy *et al.,* 2000; Fernández *et al.,* 2003; Ruff *et al.,* 2008). This is even more important in pediatric patients, as the administration of the invasive Wada-test is difficult in this population and the interpretation of its results may not be straightforward (Abou-Khalil and Schlaggar, 2002; Baxendale *et al*., 2003). However, using fMRI to examine children brings about numerous practical and methodological issues, such as intra-scanner fear (Wilke and Holland, 2008), an increased likelihood for subject motion, and issues pertaining to spatial normalization (Poldrack, Paré-Blagoev and Grant, 2002; Wilke, Schmithorst and Holland, 2002; Yuan *et al.,* 2009). Importantly, the first step is to pay special attention to task design (Wilke *et al.,* 2005, 2006; Church, Petersen and Schlaggar, 2010; Ebner *et al.*, 2011), including considerations to adapt the level of difficulty to the varying abilities of the participating age and patient groups. In particular, both frustration (“this is too hard”) and boredom (“this is too easy”) should be avoided in order to keep participants in general, and children in particular, motivated while performing a task in the scanner.

Minimizing overall time spent in the scanner is also important (Yerys *et al.,* 2009; Ebner *et al.,* 2011).

"Hemispheric dominance" is usually assessed by trying to induce activation in brain regions involved in language processing. The Experimental Pediatric Neuroimaging Group at the University of Tuebingen has previously elaborated an fMRI task battery, which is well applicable in children with average language abilities: the child-appropriate versions of the synonyms task (SYN) (Fernández *et al.,* 2001; Fernández *et al.,* 2003; Wilke *et al.,* 2006) and the vowel identification task (VIT) (Wilke *et al.,* 2006).

The SYN is a task alternating semantic judgment with letter matching, designed to allow presurgical investigation of language processing areas. This task resulted in robust left inferior frontal and posterior temporal activations in adults as originally reported by Fernández *et al.* (2001; 2003), and the same activation pattern was detected in typically developing children in previous studies applying the child-appropriate version of this task (Wilke *et al.,* 2006). The contrast of the active condition to the letter-matching part not only involves semantic decision based on retrieval of previously learned verbal information, but also reading and phonological processing (Fernández *et al.,* 2001). Semantic processing has been shown to involve areas in the left inferior frontal (IFG) and the posterior temporal gyrus (Binder *et al.,* 1996). Activation in the left IFG has been detected during making semantic decision about words (Demb *et al*., 1995; Binder *et al.,* 1996, 1997), which is in accordance with recent neurocognitive models of language processing that parcellate the IFG into parts involved in semantic, syntactic, and phonological processing (e.g., Bookheimer, 2002; Friederici, 2002; Hagoort, 2005). As stimuli are applied in a visual and not in an acoustic form, an additional grapheme-to-phoneme conversion may also contribute to activations in the left IFG (Burton, 2001).

The active condition of the VIT (VIT_{AC}) involves covert picture naming and subsequently analyzing the phonological structure of the given word to decide whether it contains the sound of the vowel "i" (always pronounced [i:] in German). In the control condition (VIT_{CC}) a pair of complex, but abstract patterns is displayed, and the participant has to decide whether the smaller one fits into the larger one "like a piece of a puzzle". Again, button presses are used to record the participant's responses. Multiple subprocesses of picture naming have been linked to the IFG and

to posterior temporal regions (for review see Duffau *et al.,* 2014). Furthermore, the IFG seems important in phonological awareness and naming (van Ermingen-Marbach *et al.*, 2013), while the posterior part of the superior temporal gyrus has been linked with the phonological output lexicon that stores the spoken representation of the words, including the phonemes they contain and their position (Butterworth, 1992; Levelt, 1992).

In the original child-appropriate version of the task battery (Wilke *et al.,* 2006), both tasks are used with a 5-second fixed stimulus onset asynchrony ([SOA] i.e., 5 seconds between the onset of two stimuli), and data analyses are performed in a block (BL) design. These tasks were shown to produce robust activations in the inferior frontal and posterior temporal language areas in the dominant hemisphere in children with average language skills (Wilke *et al.,* 2006; Lidzba *et al.*, 2011). However, children with above-average language functions found the 5‑second fixed SOA too slow, likely leading to "mind wandering" (Binder *et al.,* 1999). In contrast to this, for patients with lower language abilities the paradigm was too fast, leading to frustration and loss of compliance. Therefore, this task design was not suitable to maintain attention and keep task adherence on a desirable level for participants with language abilities outside the average range, likely resulting in weaker task-related activations and more motion artifacts.

During my PhD studies I had the opportunity to spend a fellowship in the Experimental Pediatric Neuroimaging Group and participated in the modification of this task battery. The aim of the study was to adapt the SYN and the VIT to participants with lower- as well as higher-than-average language functions, thereby broadening the applicability of this task battery and avoiding the above-mentioned confounds.

While different versions of either task could conceivably be designed, this would make direct comparisons with the original version harder. Another solution to this is the implementation within a self-paced paradigm; here, the participant individually determines the appearance of the next stimulus, as it only appears after his/her response.

There is only a small number of studies directly comparing the results of self-paced and fixed task implementations for the same cognitive task; these generally suggest that the self-paced implementation is more sensitive to detect task-related

neural correlates (D'Esposito *et al.,* 1997; Seurinck *et al.*, 2005; Tielemann *et al.,* 2005; Basho *et al.,* 2007; Krinzinger *et al.,* 2011).

In addition to the self-paced modification, the specificity of the tasks could be increased further by using an event-related (ER) analysis of the data, as it may provide a better model for the transient changes in the neural activity, decreasing residual variance in the data (Price *et al.,* 1999; Mechelli, Henson *et al.,* 2003). In the ER data analysis, each reaction can be considered as an event. Thereby, instead of identifying the brain regions participating in a conglomerate of cognitive functions active during one block, it is possible to identify the brain regions involved in the particular cognitive function of interest. A drawback of such designs is the reduced design efficiency as compared with a BL design paradigm (Mechelli, Price, *et al.* 2003).

In the language domain in particular, lateralization of activation (or hemispheric specialization) has long-since been of great interest. To this effect, a lateralization index (LI) is commonly used, comparing activation on one side of the brain with activation on the other side in one index in the range of –1 to +1 (Wilke and Lidzba, 2007). As a paradigm that yields more specificity in the detection of task-related activations must be expected to reveal more focused (and thus likely more lateralized) brain activity, assessing the lateralization of activation obtained in the BL and ER analyses may be helpful when comparing the two analytical approaches in this regard.

Based on the above-mentioned considerations, we wanted to investigate the impact of a self-paced implementation of the SYN and VIT tasks on the resulting statistical parametrical maps. Further, the impact of using a BL versus an ER analysis approach shall be explored. We hypothesized that (1) results would be comparable in the self-paced paradigm with the fixed paradigm used previously (Wilke *et al.*, 2006); (2) ER analyses will show lower design efficiency, but higher specificity of activation, and (3) lateralization of activation will differ between the two analysis approaches, with a higher degree of lateralization in the ER analysis. Additionally, we expected that the time needed for the completion of the trials would differ from the previously used fixed 5 s, when participants are allowed to perform the task in a self-paced manner.

Materials and methods

In- and exclusion criteria

As this study was aimed at methodological improvements, we felt that it was not justifiable to include participants from vulnerable populations (World Medical Association, 2013); we therefore abstained from including children. Instead, we aimed at including right-handed, healthy adults between 18 and 45 years of age. Participants were required to be in generally good health, and to be native German speakers. In addition to the usual MR-contraindications (e.g., metal implants, claustrophobia, pregnancy), participants were excluded if they had any of the followings: known disorder of the central nervous system (neurological or psychiatric), epilepsy, speech disorder, hearing impairment, or left-handedness.

Study population

20 healthy adults [age (mean ± SD): 380.1 ± 83.9 months (31.7 ± 7 years), range: 260-518 months (21.7-43.2 years), 12 females] were recruited from a database of healthy volunteers at the Department of Neuroradiology at the University of Tuebingen, as well as by public announcements. All had normal or corrected-to-normal vision. Handedness was right-dominant in all participants [Edinburgh Handedness Inventory Index (Oldfield, 1971): median: 0.91, range: 0.63-1]. The study was in accordance with the requirements of the local institutional review board, which approved the study. All participants gave written informed consent. Anatomical images were screened for structural abnormalities by an experienced neuroradiologist. All were found to be free of major anomalies; in one participant, an aberrant draining vein was seen, while in another participant, 2 nonspecific small foci of white matter hyperintensities were found. Both findings were considered nonsignificant, and all participants were retained.

Testing of language functions

Participants were assessed for language abilities by the German version of the Peabody Picture Vocabulary Test (PPVT) (Bulheller, Ibrahimovic and Häcker, 2003). During this test, participants had to match one of four pictures to a verbal characterization provided by the examiner. The advantage of this test is that it provides an opportunity for the simultaneous evaluation of vocabulary and language

comprehension. The age-corrected test percentiles of the participants ranged between 55 and 100, the median value was 97.5 percentile (for details see Table 1), reflecting above-average language abilities.

Participant ID	PPVT score	Participant ID	PPVT score
P1	88	P11	55
P2	83	P12	98
P3	99	P13	100
P4	100	P14	100
P5	76	P15	99
P6	85	P16	95
P7	99	P17	97
P8	98	P18	99
P9	99	P19	95
P10	81	P20	97

Table 1: Age-corrected test percentiles of the Peabody Picture Vocabulary Test (PPVT) of each participant. *Median value was 97.5 (range, 55-100).*

Technical implementation

In the active condition of the synonyms task (SYN_{AC}), the participant has to determine if two visually presented words are synonyms or not. In the control condition (SYN_{CC}), two nonsense letter strings are to be compared and the participant has to decide whether they are identical or not. In both conditions, responses are recorded by button presses. In the active condition of the vowel identification task (VIT_{AC}), the participant has to recognize a pictographically presented object and match a name to it (covert picture naming) and subsequently analyze the phonological structure of this word to decide whether it contains the sound of the vowel "i" (always pronounced [i:] in German). In the control condition (VIT_{CC}), a pair of complex, but abstract patterns is displayed, and the participant has to decide whether the smaller one fits into the larger one "like a piece of a puzzle". Again, button presses are used to record the participant's responses. All participants completed both tasks (SYN and VIT) in the modified version.

The modification of the tasks from the previously used, pure BL design versions (Wilke *et al.* 2006) was done to now include aspects of a mixed BL/ER design. This was achieved by keeping the overall "blocked" task layout; for example, in the first 30 seconds, only stimuli of the control condition were displayed, while in

the subsequent 30 seconds, only stimuli of the active condition were presented (and so on). However, within these blocks, the participant was able to advance stimulus presentation by a "yes" or "no" button press in each condition (conveyed via a MR-compatible two-button box [Current Design, Philadelphia, PA, USA] in the participant's right hand). This self-paced aspect on the one hand accounts for individual differences in processing speed and on the other hand allows for later ER analyses. To this effect, events were defined as beginning with the appearance of the stimulus and ending with a button press. As an aid to avoid confusion of the buttons, a little "happy green [yes] smiley" and an "unhappy red [no] smiley" were visible in the lower two corners of all displayed stimuli, along with a central fixations cross. Between two stimuli the screen went blank (with only the fixations cross and the smileys) for 0.5 second. Between two blocks, the screen turned green for 1 second to alert participants to the change of task.

Each task contained 6 blocks of the control and 5 blocks of the active condition, yielding a total scan time of 5:30 minutes. The number of trials in each condition depended on the response time of the participant (the quicker the responses, the more trials could be processed in any given condition). In order to discourage "pressing without thinking", a minimum presentation time of 0.5 second was set.

Stimulus presentation and response recording were done using Presentation (version 0.76 Neurobehavioral Systems Inc., Albany, CA, USA). Visual presentation of stimuli was achieved using MR-compatible video goggles (NordicNeuroLabs, Bergen, Norway), and MR-compatible headphones (MR-Confon, Magdeburg, Germany) were used for delivery of instructions and for noise protection in the scanner.

Data acquisition, processing and analysis

Imaging was performed on a 1.5 T whole-body MR scanner (Siemens Avanto, Siemens Medizintechnik, Erlangen, Germany) with a 12-channel head coil. An EPI-sequence was used to acquire functional series in each participant (TR = 3000 ms, TE = 40 ms, 40 axial slices, yielding a voxel size of 3 × 3 × 3 mm), covering the whole brain including the cerebellum. A T1-weighted anatomical 3D-dataset (176 continuous sagittal slices, TR = 1300 ms, TE = 2.92 ms, voxel size: 1 × 1 × 1 mm) and a gradient-echo B0-fieldmap (TR = 546 ms, $TE_{1/2}$ = 5.19/9.95 ms, 40 axial slices, voxel size: 3 × 3 × 3 mm) were also acquired. Datasets were processed using SPM8

software (Wellcome Trust Centre for Neuroimaging, London, UK), running in Matlab (Mathworks, Natick, MA, USA). The first 10 scans of each functional series (corresponding to the first block of the control condition) were rejected to allow for the stabilization of longitudinal magnetization, leaving 100 scans per series (5 blocks each of the active and the control condition). Functional images were realigned and unwarped using the individually acquired B0 fieldmap, correcting for both EPI and motion * B0 distortions (Andersson *et al.,* 2001). Following coregistration of the functional and the anatomical images, global signal trends were removed (Macey *et al.,* 2004) and functional images were smoothed with a 6 mm full width at half maximum Gaussian filter. Anatomical images were segmented using a priorless extension to the SPM segmentation algorithm as available in the VBM toolbox (Gaser *et al.,* 2007). Spatial normalization was achieved using the diffeomorphic anatomical registration approach using exponentiated Lie algebra (DARTEL; Ashburner, 2007). To this effect, standard tissue maps based on an adult control population (n = 550) were used. This procedure yields deformation fields, which may then be applied to any image in register with the anatomical.

First level (individual) statistical analyses were done in native space, using the General Linear Model (Friston *et al.,* 1995). For all analyses, the motion fingerprint (3 traces, including shifted versions) was added as covariates of no interest in order to account for signal changes attributable to motion effects (Wilke, 2012). Shifted versions were included as these were shown to explain a substantial portion of the motion-induced variance in the data (Friston *et al.,* 1996; Wilke, 2012).

In the BL design analysis, conditions were modeled in alternating blocks of 30 seconds, assuming that the task evoked a constant plateau of neural activity in the regions in question. The ER analysis was designed for closer detection of the transient activations by considering each stimulus as an event. Therefore, the onset of each event was set to each stimulus onset, and the duration of the event was defined as the time required to respond (i.e., from beginning of stimulus presentation to the button press). For both types of analyses, a canonical hemodynamic response function was used to convolve either the whole block or the individual response function.

Each statistical analysis resulted in one parameter map, ultimately leading to 4 parameter maps per participant (two for each of the two tasks). These were then spatially normalized using the deformation fields obtained before (see above) and entered into second level (group) random-effects analysis. To this effect, one-sample

t-tests were applied on a voxel-by-voxel basis to detect typical activation patterns on the group level, separately for each task and design. Age (in months), gender, handedness, and performance in PPVT were used as covariates of no interest as either parameter must be expected to affect the resulting activation pattern (Szaflarski *et al.,* 2002; Clements *et al.,* 2006; Szaflarski *et al.,* 2006). Further, the parameter maps of the BL and ER design of each task were compared by using a paired t-test. For all analyses, significance was assumed at a voxelwise $p \leq 0.05$, FDR-corrected for multiple comparisons (Genovese, Lazar and Nichols, 2002) and an additional cluster-level FWE-correction at $p \leq 0.05$ (Friston *et al.,* 1994).

Assessment of lateralization

In this study we used the weighted mean from a bootstrapping approach (Wilke and Schmithorst, 2006) as implemented in the LI-toolbox (Wilke and Lidzba, 2007), with default settings (no optional steps, bootstrap sample size: 25%, minimum bootstrap sample size: five voxels, maximum bootstrap sample size: 10,000 voxels). This approach is robust to outliers and avoids the threshold dependency inherent to other approaches. Based on previous studies (Price, 2000; Riecker *et al.,* 2000; Szaflarski *et al.,* 2002; De Smet *et al.,* 2013), we decided to specifically investigate the frontal lobe and the cerebellum, using slightly modified versions of the masks coming with the LI-toolbox in order to account for the lesser smoothing employed here. These masks are designed to safely cover the respective structures while excluding adjacent brain or non-brain tissue. As before (Wilke *et al.,* 2005, 2006; Ruff *et al.,* 2008), values of $-0.2 < LI < 0.2$ were considered bilateral; values ≤ -0.2 were considered right-dominant, while values ≥ 0.2 were considered left-dominant. Owing to non-normally distributed values, differences between lateralization indices (BL vs. ER design) were assessed using the two sample non-parametrical Mann–Whitney-U test, and significance was assumed at $p \leq 0.05$. The equality of the LI variances (BL vs. ER) was examined by Levene's test, and significance level was set to $p \leq 0.05$.

Design efficiency

Conceptually, design efficiency reflects the reliability of a model to actually estimate the parameters, and thus is a measure of model sensitivity. It is inversely related to the estimator variance and was used before to compare different design

implementations (Mechelli, Price *et al.,* 2003). A well-known drawback of an ER design is its lower design efficiency. In order to assess the magnitude of this effect, design efficiency was calculated here for every participant and both designs, using the approach described by Mechelli, Price *et al.* in 2003. To further evaluate the reliability of the ER design, the mean number of activated voxels at a more liberal, individual threshold of $p \leq 0.001$, uncorrected, was computed and compared in left frontal and right cerebellar regions in both designs and in both tasks, using the custom-defined masks of the LI analysis. The difference was again evaluated by using the Mann-Whitney-U test, assuming significance at $p \leq 0.05$.

Results

Group activation maps (one sample t-test)

The second-level random-effects analysis of the BL and the ER designs showed significant left inferior frontal and left posterior temporal activation clusters, as well as mainly right cerebellar activations in the active condition of both tasks, in both designs (Figure 1; Figure 2, left panel).

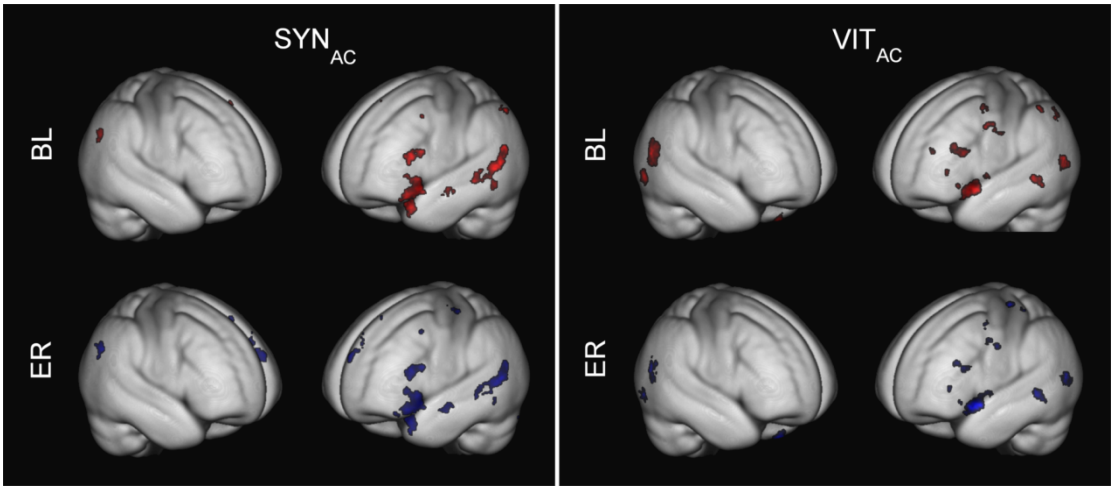

Figure 1: Group activation maps of the block (BL, upper row) and event-related (ER, lower row) analyses of the active condition of the synonyms (SYN_{AC}, left panel) and vowel identification (VIT_{AC}, right panel) tasks*, obtained by one-sample t-test and rendered on a gray matter template. All activations are significant at $p \leq 0.05$, FDR- corrected for multiple comparisons on voxel-level, and at $p \leq 0.05$, FWE-corrected on cluster level. Note robust left fronto-temporal activation clusters elicited by both tasks in both designs.*

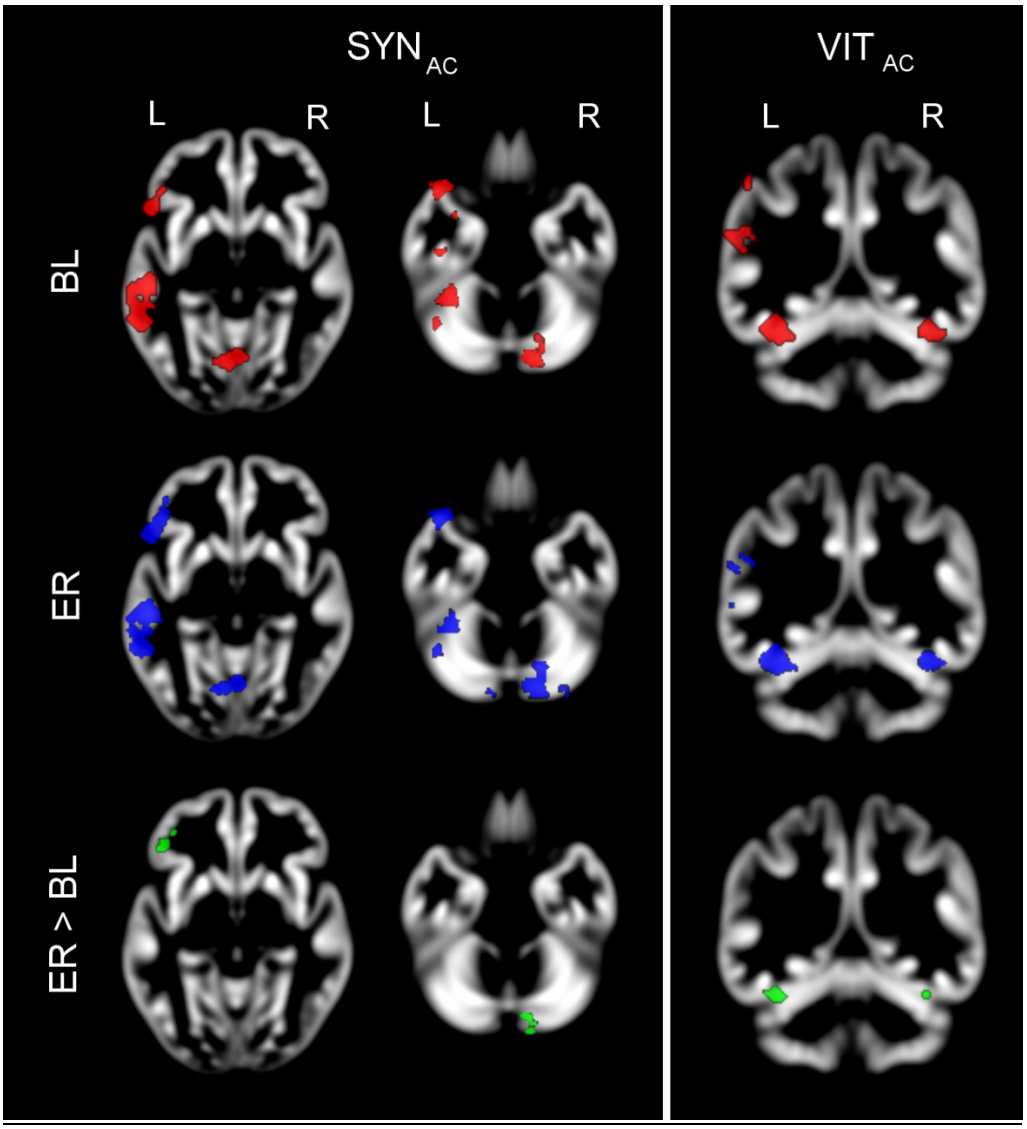

Figure 2: Group activation maps of the block (BL, upper row) and event-related (ER, middle row) analyses of the active condition of the synonyms (SYN_{AC}, left panel) and vowel identification (VIT_{AC}, right panel) tasks and their difference (lower row) *Left panel: Frontal (left column) and cerebellar (right column) activations in the block (BL, upper row) and event-related designs (ER, middle row) of the synonyms task (SYN_{AC}) and their difference (ER > BL, bottom row) as detected by the paired t-test, overlaid on sections of a gray matter template. All activations are significant at $p \leq 0.05$, FDR-corrected for multiple comparisons on voxel-level, and at $p \leq 0.05$, FWE-corrected on cluster level. Note more prominent activation in left inferior frontal and right posterior cerebellar regions (bottom row). Orientation is neurological (i.e., left = left). Right panel: Activation in the lingual gyrus in the active condition of the vowel identification task (VIT_{AC}) in the block (BL, upper row) and event-related designs (ER, middle row) and their difference (ER > BL, bottom row) as detected by the paired t-test, overlaid on sections of a gray matter template. Note that the ER design detected significantly (at $p \leq 0.05$, FDR-corrected for multiple comparisons on voxel-level, and at $p \leq 0.05$, FWE-corrected on cluster level) stronger activation bilaterally in the lingual gyrus. Orientation is neurological (i.e., left = left).*

Comparison of block and event-related design (paired t-tests)

When comparing the block and the event-related design (BL > ER) of the SYN task, there were no significant differences in activation in key language areas (data not shown). In the inverse comparison (ER > BL), the ER analysis resulted in

significantly stronger activations in left inferior frontal region and in the posterior lobe of the right cerebellum (Figure 2, left panel).

There were no significant differences in language-related brain regions in the BL > ER comparison of the VIT (data not shown). In the inverse comparison (ER > BL), a stronger activation was found in the lingual gyrus bilaterally (Figure 2, right panel).

Lateralization

Similar lateralization patterns were found in the BL and ER designs in both tasks (Figure 3). In the SYN task, frontal activation was left-dominant (LI_{BL}: median: 0.58, range: -0.25 to 0.84; LI_{ER}: median: 0.54, range: –0.25 to 0.82), while cerebellar activations showed right dominance (LI_{BL}: median: –0.41, range: –0.81 to 0.84; LI_{ER}: median: –0.44, range: -0.81 to 0.8). In the VIT, similar left frontal and right cerebellar dominance was detected (frontal: LI_{BL}: median: 0.56, range: –0.05 to 0.85; LI_{ER}: median: 0.52, range: 0.00 to 0.85; cerebellar: LI_{BL}: median: –0.41, range: –0.82 to 0.5; LI_{ER}: median: –0.4, range: –0.79 to 0.29). There was no significant difference in lateralization between task designs, in either region (all Mann-Whitney-U with $p > 0.05$). The observable variance of results was also comparable (all Levene's $p > 0.05$).

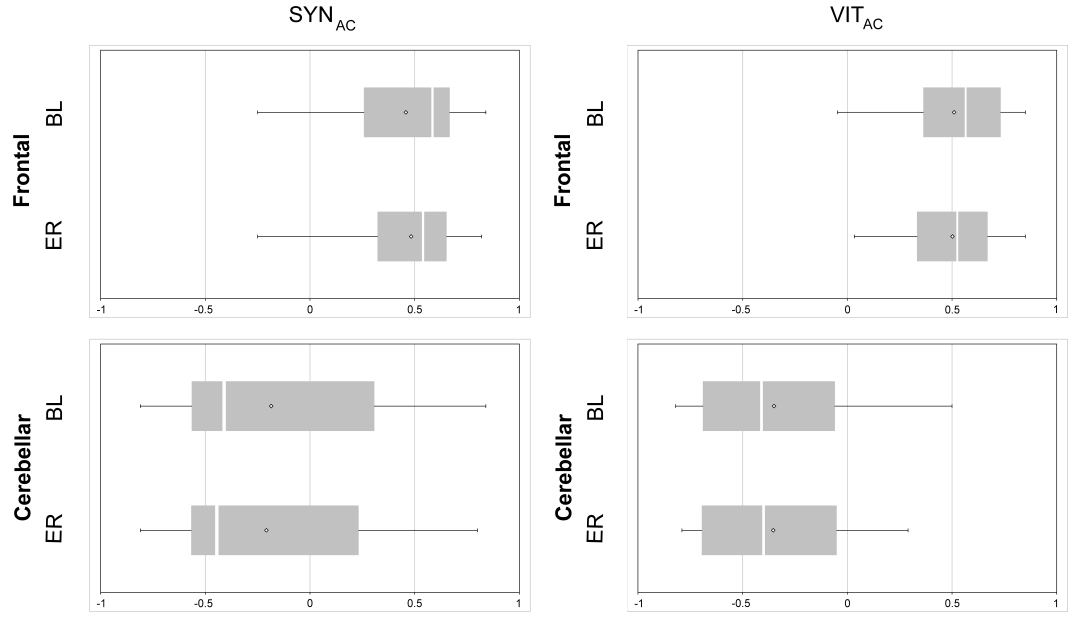

Figure 3: Box whisker plots of the lateralization indices in the frontal lobe (upper plots) and the cerebellum (lower plots) in both tasks (SYN_{AC}, left, and VIT_{AC}, right) and both designs [block (BL) and event-related (ER)]. *Note consistent left lateralization in frontal regions with crossed cerebellar lateralization. Neither difference between the two designs reached significance.*

Participant performance

In both tasks, the average time required for stimulus processing ranged from 1.25 to 1.79 seconds, more than 2.5-times shorter than the fixed 5-second SOA in the original versions. With regard to the overall number of trials processed (reflecting task difficulty), both tasks were very similar. Stimuli in the control condition were processed slightly slower, again very similarly in both tasks (Table 2). Reaction times were significantly faster in the active condition (Wilcoxon rank sum test, $p < 0.01$), but the number of trials was not significantly different for either task (Mann-Whitney-U test, $p > 0.05$ for both tasks).

	Synonyms task				**Vowel identification task**		
Condition	Mean RT [s]	Mean # of trials	Incorrect responses		Mean RT [s]	Mean # of trials	Incorrect responses [a]
Active	1.25 ± 0.48	81.7 ± 12.96	2.2 ± 1.77		1.29 ±0.60	80.2 ± 14.85	4.15 ± 3.36
Control	1.79 ± 0.74	74.95 ±13.97	3.2 ± 3.4		1.68 ±1.04	78.05 ± 21.17	4.45 ± 3.83

Table 2: Response times (RT) for all participants (n = 20) for both tasks and both conditions. [a] *Note that an "incorrect" answer in the VIT may in rare cases reflect a less common, but equally valid solution found by the participant: when the image of a "ship" is shown, the participant can call this "boat", so the answer "no" would be correct.*

Design efficiency, mean number of activated voxels

As expected, design efficiency was lower for the ER implementation, with a mean of 66.19 ± 5.02% for the SYN task and a mean of 65.78 ± 9.44% for the VIT task (when related to the respective BL design implementation). The difference in the raw values was significant for both tasks (Mann-Whitney-U test, $p < 0.01$). However, the mean number of voxels activated was not different in the left frontal lobe or the right cerebellum, for the SYN (722.2 ± 711.45 [BL] vs. 694.6 ± 709.2 [ER] and 115.3 ± 170.53 [BL] vs. 112.85 ± 171.98 [ER]) or the VIT (702.85 ± 664.43 [BL] vs. 598.4 ± 571.75 [ER] and 91 ± 152.92 [BL] vs. 85.3 ± 125.11 [ER]). Neither of these differences in the numbers of activated voxels reached significance (Mann-Whitney-U, all $p > 0.05$).

Discussion

For the purpose of presurgical determination of language dominance, the Experimental Pediatric Neuroimaging Group at the University of Tuebingen has

previously established the child-appropriate versions of the synonyms (SYN) and the vowel identification tasks (VIT). These tasks have been successfully used to examine children with average and slightly below-average language abilities (Wilke *et al.*, 2006; Everts *et al.,* 2009; Wilke *et al.,* 2010; Ebner *et al.* 2011; Wilke *et al.*, 2011; Zsoter, Staudt and Wilke, 2012). However, the application of these tasks often proved to be problematic in children with language functions outside the average of the scale. Therefore, the main motivation for this work was to modify these tasks in a way to make them more appropriate for participants with a wider range of language abilities.

Effects of adding a self-paced component

The self-paced modification of both tasks resulted in a highly specific and selective pattern of activation in key language areas, such as left inferior frontal and left posterior temporal regions, as well as right posterior cerebellar activations (Figure 1; Figure 2, left panel). This activation pattern confirms previous results (when using a fixed SOA) very nicely (Wilke *et al.,* 2006; Ebner *et al.,* 2011; Lidzba *et al.,* 2011), demonstrating that the overall pattern does not change as a function of said modification.

There is a considerable (almost 2.5-fold) difference between the fixed 5-second SOA used previously and the average reaction time of our participants in the here-described self-paced modification. This indicates that in the unmodified, fixed SOA version of the tasks, our participants would have required less than half of the provided 5 seconds to complete a given trial of the task, while they would have spent the remaining time passively waiting for the next stimulus. This underlines the advantage of using a self-paced paradigm, as subjects can perform at their own pace. This passive waiting harbors the danger of "mind-wandering", leading to decreased task-related activations or even more task-related deactivations (Binder *et al.,* 1999; Daselaar, Prince and Cabeza, 2004). Furthermore, the self-paced approach is quite intuitive, since it gives the impression of a slide projector (i.e., the next slide appears when a button is pressed) as opposed to the original approach with fixed SOA, which some children found confusing, since "nothing happened" when they pressed the button. For children in particular, continued (visual) task engagement has been shown to decrease the occurrence of motion artifacts (Poldrack *et al.,* 2002;

Yuan *et al.,* 2009). All of this argues in favor of using a self-paced approach for participants with above-average language abilities.

On the other hand, frustration will be induced if trials are too fast for participants with below-average language abilities, likely reducing subsequent task adherence and compliance. In those participants, even though fewer stimuli may be processed as in a design with a fixed SOA, the time spent "on the task" constructively must be expected to be higher. Further, the self-paced implementation provides an effective way to monitor task performance and adherence, which is often a cause of concern in fMRI studies requiring covert responses (Gaillard *et al.,* 2003; Szaflarski *et al.,* 2006).

The above-described advantages argue in favor of the assumption that the self-paced modification of the SYN and VIT tasks may render them suitable for the investigation of a broader participant population (for a further discussion of this aspect, see the Implications for pediatric fMRI studies section).

Comparison of specificity between block (BL) and event-related (ER) design

The comparison of the BL and ER design analyses was performed based on the hypothesis that the conventional BL design approach will reflect the sustained activity while performing the task. In contrast to this, an ER processing approach may allow focusing on the transient neural activity elicited by the stimuli (Petersen and Dubis, 2012); this model may thus be a better representation of task-related signal changes and yield a more specific activation pattern.

In the case of the SYN task, the ER analysis revealed significantly stronger activations in left inferior frontal and right posterior cerebellar areas than in the BL design (Figure 2, left panel). These activations were robust enough to survive the double correction for multiple comparisons applied here. It is also important to note that the difference between the BL and the ER designs was only detected in these language-related regions and that no significant differences were observed in the inverse contrast (BL > ER), further underlining the added specificity the modified analysis approach seems to provide.

In case of the VIT, the ER analysis yielded significantly stronger activation bilaterally in the lingual gyrus (Figure 2, right panel), which has a role in semantic processing, object recognition and associative encoding (Hinojosa *et al.,* 2000; Karnath *et al.,* 2009). In post-hoc exploratory analyses of the ER > BL contrast at a

more lenient $p = 0.001$, uncorrected, stronger activation was also found in left inferior-frontal and right cerebellar regions (data not shown), similar to the pattern seen in the SYN and thus weakly suggesting a higher specificity of the ER implementation also for this task.

The fact that the ER analysis found more prominent task-related activations in core language areas is surprising as such approaches have inherently lower design efficiency (Mechelli, Henson *et al.,* 2003). This was also found in our analyses, with the efficiency of the ER analyses being about $^1/_3$ lower. However, this was not accompanied by a significant reduction in the number of activated voxels on the individual level, suggesting that this reduced design efficiency was not detrimental to sensitivity in our participants. In fact, in both the BL and ER implementations, all subjects showed suprathreshold activation in the left frontal lobe in each task irrespective of the analytical approach, illustrating that both tasks robustly elicit activation in core language regions. This stability of activation on the individual level, while not the focus of this study, is an important prerequisite for fMRI tasks aimed at clinical applications (Church *et al.,* 2010; Khorrami *et al.,* 2011; Zsoter *et al.,* 2012).

Lateralization

The left frontal and right cerebellar lateralization pattern was constant across both tasks and analysis methods. This consistent lateralization pattern corresponds well to the results reported in previous studies with the fixed SOA versions of the tasks (Wilke *et al*., 2006; Lidzba *et al.,* 2011), therefore again supporting the notion of a similar reliability of the self-paced implementation to assess lateralization of the language processing network. Although we hypothesized that the ER design may yield a higher degree of lateralization due to its higher specificity, only a tendency to provide a higher consistency (lower variability) of lateralization seemed to be present, but this difference was not statistically significant.

There is increasing evidence in the literature about the role of the cerebellum in higher cognitive functions, such as language (Leiner, Leiner and Dow, 1989; Grodd, Hülsmann and Ackermann, 2005; De Smet *et al.,* 2013). In particular, a consistently contralateral pattern of cerebellar activation during covert speech has also been shown previously (Riecker *et al.,* 2000; Jansen *et al.,* 2005). As our tasks include either reading of words and semantic (in the SYN) or phonological analyses (in the VIT), they may have induced internal, covert articulation. Our findings therefore are

in accordance with these works, as the detected cerebellar activation was mainly localized to the posterior lobe of the right cerebellum, and a clear tendency can be observed in our results that cerebellar and frontal activations appear in a contralateral fashion (Figure 3). Importantly, this crossed pattern was previously also observed in participants showing reorganized language following early left-hemispheric brain lesions (Lidzba *et al.,* 2008). While not formally investigated here due to a lack of participants with such an atypical activation pattern, this suggests that a combined assessment of both frontal and cerebellar regions may increase the reliability of the verdict of "hemispheric dominance" on the individual level.

Implications for pediatric fMRI studies

Successfully performing language fMRI in children is challenging on several levels; among them, the design of appropriate tasks is of utmost importance (Wilke *et al.,* 2005, 2006; Church *et al.,* 2010; Ebner *et al.,* 2011). Particularly in the clinical setting, the intersubject variability in a patient population may be increased substantially due to age or disease-related factors determining the level of cooperation (Poldrack *et al.,* 2002; Kotsoni, Byrd and Casey, 2006; Yerys *et al.,* 2009; Yuan *et al.,* 2009). Developing tasks that can be used effectively in this setting is an important challenge, and based on our here-reported results, the self-paced implementation in combination with an ER design may offer an interesting alternative.

Possible limitations

A potential limitation of self-paced group studies is that some participants spend more time on one condition than others, harboring the danger of confounding group results when including an inhomogeneous group of participants (Krinzinger *et al.,* 2011) or two conditions with differing levels of difficulty. However, the number of presented stimuli did not show high intersubject fluctuations in our cohort, with all participants showing a high performance (Table 2); we therefore do not think that behavioral variability is a relevant confound in this work. Furthermore, our mixed BL/ER implementation ensures that the overall time spent on each condition is inherently constant in all participants, which is an improvement over a pure self-paced, ER implementation and thus an "added bonus" of this approach.

During task design, attention should be paid that the required number of button presses should be kept nearly equivalent between the active and control conditions to prevent cerebellar motor activations from confounding the results (Pillai *et al.,* 2004). Regarding our study, since no difference was detected between the activations in the primary motor area on either contrast between the two designs (BL > ER or ER > BL), it is not likely that the right cerebellar activation seen more prominently in the ER design were due to motor activity. Also, the number of responses was similar between the active and the control conditions (Table 2), again arguing in favor of rather "balanced" designs (in terms of the level of difficulty over conditions).

For fMRI studies, the "ideal" sample size to achieve reliable and reproducible results continues to be an important consideration. It has been shown that a group size of n ~20 is appropriate to achieve acceptable reliability of the findings (Thirion *et al.,* 2007). Furthermore, the activations reported in this study were robust enough to survive the rigorous correction and were obtained without masking and small volume correction, further arguing in favor of the robustness of these effects (Friston, 2013).

The comparison of the self-paced modification of the tasks with the original versions with fixed SOA in the aspect of applicability was only indirectly possible in our study, as we only applied the former here, and the focus of this work was the comparison of the BL vs. ER analytical approaches of the self-paced modification implemented in a mixed BL/ER acquisition. While direct comparisons may have provided more insight into the differences in the applicability of the two designs, this would bring about issues of training and recognition effects.

When assessing task performance and participant's abilities (cf. Table 1 & 2), it is apparent that the variance in both parameters was small, and participants with low language abilities, or low task performance, were severely underrepresented in this sample; in other words, there was a strong ceiling effect. We therefore abstained from investigating a possible interrelation of either factor with fMRI activation levels, as this would not yield meaningful (in terms of representative and generalizable) results.
It has to be noted that the tasks applied in this study in adult participants were child-appropriate ones (as the VIT was originally designed for children, and the original SYN task published by Fernández *et al.* in 2001 has been previously modified to be suitable for pediatric studies by omitting words deemed too difficult for children

[Wilke *et al.,* 2006]). This inherently increases the risk of performance-related bias in the results. Expectedly, children with above-average and even more with below–average language abilities would find these tasks more difficult than our adult participants, and therefore would likely show lower performance. Future studies are needed on both groups of minors to set magnitude for the extent of this effect.

Investigation of the brainstem with diffusion tensor tractography

Introduction

Basics of diffusion tensor imaging (DTI)

Diffusion tensor tractography (DTT) is a method based on DTI. DTI is sensitive to the diffusion of water molecules. The rate of diffusion in free water is the same in all directions (i.e., isotropic), while in white matter it is higher along fibers, than perpendicular to them (anisotropic diffusion). Therefore, in white matter, the principle direction of diffusion corresponds with the main fiber orientation within a given voxel (Stejskal and Tanner, 1965; Basser *et al.*, 1994a, b; LeBihan *et al.*, 2001). The diffusion process can be modeled by an ellipsoid (or tensor) mathematically represented by a 3 × 3 symmetric matrix (Basser *et al.*, 1994a, b). Using this information, DTT is capable of depicting white matter microstructure *in vivo* (Mori *et al.*, 1999; 2002), which is not possible by conventional imaging (Witwer *et al.*, 2002).

DTT algorithms can be divided into deterministic and probabilistic methods. Deterministic tractography takes a single fiber orientation per voxel into account and propagates streamlines in a stepwise fashion until meeting any of the stopping criteria (curvature limit, non-brain tissue, low anisotropy values) (Conturo *et al.*, 1999; Mori *et al.*, 1999; Basser *et al.*, 2000; Mori *et al.*, 2002; Lazar *et al.*, 2003). Probabilistic tractography determines a probabilistic distribution of fiber orientations within a voxel, therefore provides possibility to investigate probabilistic connectivity of different brain areas (Behrens *et al.*, 2003b). In contrast to deterministic algorithms, probabilistic tractography is not limited by low fractional anisotropy values

(e.g., in gray matter) (Behrens *et al.*, 2003a; Jones, 2008), therefore it can identify subcortical nuclei based on their cortical connections (Behrens *et al.*, 2003b).

DTI is increasingly used in cases when the spatial relationship of an eloquent brain area and a pathology has to be determined (e.g., Pagani *et al.*, 2005; Philips *et al.*, 2005; Helton *et al.*, 2006; Chen *et al.*, 2007a, b; Lui *et al.*, 2007; Helton *et al.*, 2008; Giussani *et al.*, 2010; Kovanlikaya *et al.*, 2011; Prabhu *et al.*, 2011; Kis *et al.*, 2014; Ulrich *et al.*, 2014). For example, in brain tumor cases, it can be of significant help in the decision of operability, or even in preoperative planning. Probabilistic tractography is also suitable for the quantitative investigation of anatomical connectivity (Lazar, 2010) between brain regions either in healthy individuals or in various disease states (injuries, psychiatric illnesses, cerebral malformations, etc.). This information can also be used to monitor disease or to support therapeutic decisions.

Connectivity-based brainstem segmentation

The brainstem is a compact anatomical structure, densely packed with important cranial nerve nuclei and vegetative centers surrounded by ascending, descending and crossing fiber tracts. Its main functional regions integrate important components of systems regulating cognitive-, motor-, and sensory functions, and consciousness. Due to its complexity, small size and fairly homogeneous appearance on conventional MRI, in vivo examination of brainstem structures is still a challenging field of modern neuroimaging.

Most studies using diffusion MRI to investigate the normal anatomy or pathologies of the brainstem have either used color-coded vector maps (Stieltjes *et al.*, 2001; Golay *et al.*, 2002; Nagae-Poetscher *et al.*, 2004; Salamon *et al.*, 2005; Habas and Cabanis, 2007; Kamali *et al.*, 2009, 2010; Soria *et al.*, 2011; Aggarwal *et al.*, 2013) or diffusion tractography (Stieltjes *et al.*, 2001; Nagae-Poetscher *et al.*, 2004; Wakana *et al.,* 2004; Newton *et al.,* 2006; Ramnani *et al.*, 2006; Habas and Cabanis, 2007; Upadhyay *et al.*, 2008; Kamali *et al.*, 2009; Hodaie *et al.*, 2010; Hong *et al.*, 2010; Kamali *et al.*, 2010; Edlow *et al.*, 2012; Aggarwal *et al.*, 2013; Ford *et al.,* 2013; McNab *et al.,* 2013; Yeo *et al.,* 2013; Meola *et al.*, 2016). Most tractography studies at least partially relied on anatomical landmarks within the brainstem. However, when pathological lesions or space occupying tumors are present, color-coded vector maps

can be hard to interpret and identification of anatomical landmarks is difficult and unreliable.

Behrens *et al.* (Behrens *et al.,* 2003b) were the first to use probabilistic tractography and Bayesian techniques to perform connectivity-based segmentation of the thalamus. This method classifies each thalamic voxel according to the ipsilateral cortical region with which it shows the highest connection probability; and the specific connectivity pattern of each thalamic nucleus allows determination of its location. Based on this principle, connectivity-based segmentation offers parcellation of a cortical or subcortical area without a priori information on the distribution of the connecting areas and without reliance on anatomical landmarks within the cerebral structure or region of interest.

In my PhD work my aim was to elaborate an application of connectivity-based segmentation for the identification of the most important functional subregions of the brainstem. Such a method would have the benefit of eliminating the need for anatomical landmarks within the brainstem to detect these functional subregions. Thereby it could be applied in diseases when a pathology (tumor, injury, demyelination, etc.) causes distortion of the normal anatomy.

The main functional systems in the brainstem that this work was focused on regulate cognitive-, motor-, and sensory functions and consciousness: 1, frontopontine pathways, which represent connections to the prefrontal cortex playing a decisive role in cognitive processes (Leiner *et al.,* 1991; Ramnani *et al.,* 2006; Krienen and Buckner, 2009), 2, corticospinal and corticobulbar tracts (CST/CBT), being the efferent pathway of the primary motor cortex, 3, sensory connections involving the spinothalamic tracts and the medial lemniscus and 4, reticular formation being an important component of the ascending reticular activating system (ARAS), which controls arousal.

The results of the connectivity-based brainstem segmentation performed on a group of healthy adults were examined for correspondence with the known anatomy (histological sections and with a microscopic atlas [Nieuwenhuys *et al.,* The human central nervous system, 3rd edition, Berlin, Springer Verlag, 1988, Figures 99 and 103, reproduced with permission]), and reproducibility on the group level. Furthermore, my aim was to identify potential biomarkers (characteristic subregion-specific changes detected in the connectivity and fractional anisotropy [FA] values along the rostrocaudal axis of the brainstem) that may be of significant help in

the diagnosis and prognosis estimation of brainstem pathologies (e.g., pediatric cerebral malformations, brainstem injury due to head trauma, tumors, demyelinating disorders, etc.).

The results of this study can be divided into two distinct parts: the localization of the above mentioned functional brainstem subregions and their quantitative assessment to find potential biomarkers. Another PhD thesis is based on the first part, namely the localization and identification of the functional subregions by connectivity-based segmentation, therefore the method itself and the first part of the results will not be discussed in details in this PhD thesis. On the other hand, the identification of these subregions is the prerequisite of the quantitative assessment, therefore brief description of the method is provided in this thesis as well.

Materials and methods

Study population

20 healthy participants were enrolled in the study (age [mean ± SD]: 31.7 ± 7 years, range: 21.7−43.2 years, 12 females). None of them had any previous history of neurological or psychiatric disease. On the structural MRI images, no abnormalities were detected, as verified by a neuroradiologist. The study was approved by the Institutional Review Board. Written informed consent was obtained from all subjects.

Data acquisition

Scanning was conducted on 1.5 T GE Signa Excite scanner with an eight-channel head coil and maximum gradient strength of 33 mTm^{-1}. High resolution T1-weighted scans (3D IR-FSPGR: TR/TE/TI: 10.3/4.2/450 ms, flip angle: 15°, ASSET, FOV: 25*25 cm, matrix: 256*256, slice thickness: 1 mm) and diffusion-weighted images (DTI: TR/TE: 11500/97.4 ms, flip angle: 90°, FOV: 23*23 cm, matrix: 96*96, slice thickness: 2.4 mm, voxel size: 2.4 mm isometric, the ASSET option was used to decrease image distortions of the posterior fossa and acquisition time, number of excitations: 2, b = 1000 s/mm^2) in 60 independent directions and six non-gradient sets (b = 0 s/mm^2) were acquired. Scans covered the whole brain. Total scan time took 35-40 minutes per subject. All images were acquired parallel to the anterior-posterior commissure line.

Data preprocessing

MRI data were preprocessed using tools of the FMRIB Software Library (FSL, v5.0 [Smith *et al.,* 2004; Woolrich *et al.,* 2009; Jenkinson *et al.,* 2012]; FDT, v3.0, [Behrens *et al.,* 2003a, b]; Oxford Centre for Functional MRI of the Brain [FMRIB], UK; www.fmrib.ox.ac.uk/fsl) as it was previously described by Behrens *et al*. (Behrens *et al.,* 2003b). MRICron was used to convert DICOM images to NIFTI format (Rorden *et al.,* 2007). Eddy current and head motion correction were done, followed by skull stripping (Smith, 2002), reconstruction of diffusion tensors, and estimation of diffusion parameters. Transformation matrices between the structural, diffusion and standard (Montreal Neurological Institute, MNI152 2 mm brain) spaces were obtained by FMRIB's linear registration tool FLIRT (Jenkinson and Smith, 2001; Jenkinson *et al.,* 2002). Individual FA maps were registered to the MNI standard brain by using the above described transformation matrices. Next, individual FA maps were mathematically summed and averaged to create a group FA map (Pagani *et al.,* 2005).

Selection and definition of masks

In order to identify the four brainstem subregions (frontopontine, motor and sensory pathway, reticular formation) within the pontomesencephalic portion one seed and six target masks were used. The pontomesencephalic portion of the brainstem was defined as the seed mask in this study. Target masks were the following: a coronal single-slice section of the left (1) and right (2) anterior limb of the internal capsule (ALIC) to detect frontopontine connections (Kamali *et al.,* 2010), an axial single-slice section of the left (3) and right (4) posterior limb of the internal capsule (PLIC) to trace the CST/CBT (Stieltjes *et al*., 2001; Wakana *et al.,* 2004; Ulrich *et al.,* 2014), the bilateral sensory (Ulrich *et al.,* 2014) (5) and medial (6) thalamus to find the main ascending sensory pathways (medial lemniscus, spinothalamic pathways) and the reticular formation, respectively. Drawing of the masks took 1 hour per subject.

Probability distribution maps of the subregions and brainstem connectivity maps derived by hard segmentation at the individual and group level

Probabilistic tractography was performed with default settings of the FMRIB Diffusion Toolbox (Behrens *et al.,* 2003a, b) to generate probability distribution maps (PDM) of the six subregions (left and right frontopontine, left and right motor

subregions, sensory pathways and reticular formation) at the individual and group level. Then connectivity maps (CM) were created from the PDMs by hard segmentation (Behrens *et al.,* 2003b) for all participants individually and a group CM as well. The CM consisted of six connectivity defined regions (CDR), corresponding to the location of the PDMs. To eliminate low-probability connections, eight different threshold levels (1%, 5%, 10%, 15%, 20%, 25%, 35% and 50%) were tested from which the 25% seemed to be the most anatomically plausible (data not shown). Therefore, for later analyses this threshold level was arbitrarily chosen.

Intersubject variability maps (Ciccarelli *et al.,* 2003; Johansen-Berg *et al.,* 2005; Newton *et al.,* 2006) showing the case-to-case anatomical variability of each PDM were created the following way: individual PDMs were registered to standard space, then thresholded at 25%, binarized and summed. This way, voxel values within the intersubject variability maps represented the number of subjects with connection in that given voxel. In order to remove those voxels that only showed connectivity in a small number of subjects, we applied a threshold of 6/20 subjects to these maps.

Total analysis time from data acquisition to the completion of the connectivity-based brainstem segmentation took 24-48 hours per subject on an Apple Mac Pro, 2x2.4 GHz 6 Core Intel Xeon processor, 12 GB 1333 MHz DDR3 RAM (Apple Inc., California, USA).

Quantitative assessment of the reproducibility of the connectivity-based brainstem segmentation

First, we wanted to quantitatively evaluate the consistency of the results of the connectivity−based brainstem segmentation across our subjects. As the PDMs are elongated, mainly rostrocaudally oriented structures, the center of gravity of the connectivity values (CoG_{conn}) in each axial slice of the PDMs were chosen for the comparison of the individual results. To exclude collateral connections from the PDMs and retain only those voxels that are incorporated in the segmented CDRs as well, we applied masking of the PDMs before performing the calculation of the CoG_{conn} coordinates. For this purpose, a group probability mask was created for each subregion. To this end, individual PDMs were registered to standard space, thresholded at 25% and hard segmentation was performed. From the derived individual CMs in standard space the six different CDRs were separated. The 20 individual separated CDRs of the same subregion were binarized and summed

to create a group probability mask of the given CDR. The midsagittal plane (x = 0, all coordinates are displayed in MNI152 2 mm space) was used for splitting the sensory and the reticular group probability masks to left and right sensory and reticular group masks, respectively. Both the left and right motor group probability masks were thresholded at 14/20 subjects (a high threshold level was needed to exclude remaining dorsal collaterals and to keep the CST/CBT regions only), and the left and right frontopontine, sensory and reticular group probability masks were thresholded at 6/20 subjects (that is, those voxels that were incorporated in the given CDR of less than 6 subjects were excluded) (Figure 4).

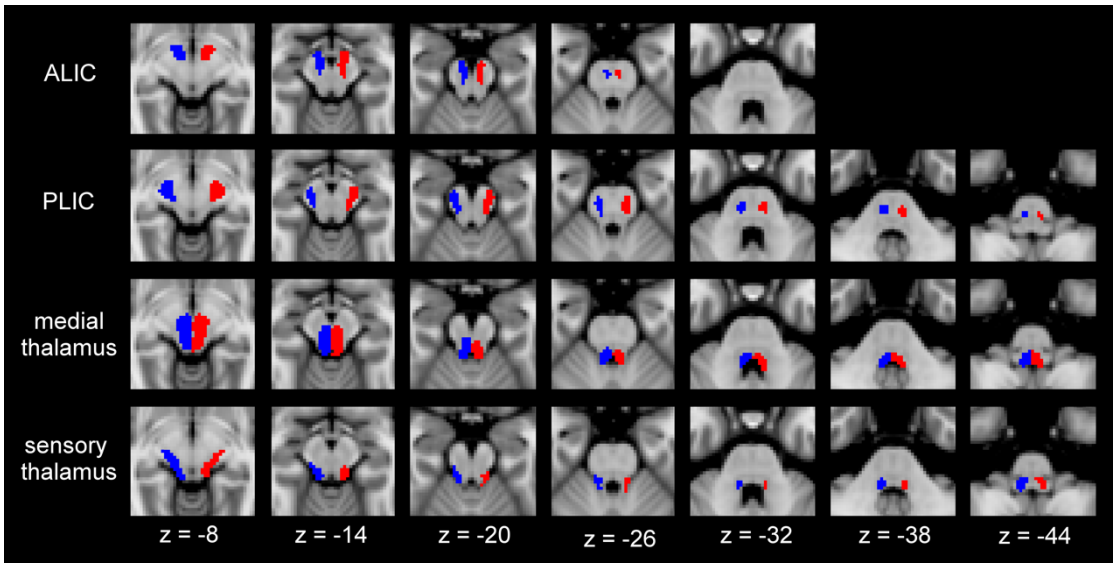

Figure 4: Group probability masks overlaid on axial slices of the MNI152 2 mm brain from z = −8 to z = −44. *Color-coding: red – left, blue – right. The first row shows the frontopontine group probability masks (extracted from the probability distribution map seeded from the anterior limb of the internal capsule [ALIC]). The second row shows the motor group probability masks (extracted from the probability distribution map seeded from the posterior limb of the internal capsule [PLIC]). The third row shows the reticular group probability masks (extracted from the probability distribution map seeded from the medial thalamus). The fourth row shows the sensory group probability masks (extracted from the probability distribution map seeded from the sensory thalamus). Please note that the collateral connections of the specific regions are not present here when compared to the intersubject variability maps (see later as Figure 5). Orientation is radiological (i.e., left = right).*

We used the group PDM as a reference for the measurement of the distances of the individual CoG_{conn} locations. As the reticular formation is a C-shaped region located symmetrically with respect to the midline of the brainstem, it is not possible to identify a single CoG_{conn} value in it. For this reason, the group and individual reticular PDMs were split in the midsagittal plane (x = 0), and the CoG_{conn} was separately determined for both sides. The unthresholded group and individual PDMs registered in standard space were masked with the corresponding group probability mask. In the next step, we used fslstats to define the x, y, z coordinates of the CoG_{conn} of the

masked group PDMs and the corresponding masked individual PDMs in each axial slice from z = - 10 to z = - 48, and calculated their distance in mm.

Comparison of segmentation results to microscopic anatomy and anatomical reference material

The correspondence between the known microscopic anatomy and the brainstem segmentation results was tested on a two step basis. Distinct anatomical structures were identified by an experienced neuroanatomist and the help of the corresponding sections of a neuroanatomy atlas (Nieuwenhuys *et al.,* The human central nervous system, 3rd edition, Berlin, Springer Verlag, 1988, Figures 99 and 103. Reproduced with permission.). The histological sections were obtained from a single subject (41-year-old male without history of neurological disorders or brain injury) and stained for myelin and for cells (courtesy of the Department of Anatomy, University of Szeged, Hungary). Corresponding sections of the neuroanatomy atlas were overlaid on the histological images and sections of the MNI152 1 mm standard brain. The results of the connectivity-based brainstem segmentation were visually compared with the underlying anatomical structures. The anatomical structures used for comparison were the followings: frontopontine tract (frontopontine CDR), corticospinal tract and occipitoparietotemporopontine tract (motor CDR), medial lemniscus, and spinothalamic tract (sensory CDR), central tegmental tract, superior cerebellar peduncle, dorsal longitudinal fasciculus (reticular CDR).

Assessment of subregion-specific quantitative measures (connectivity, FA)

We investigated the relationship between the connectivity values of the PDMs and the corresponding FA values, and whether characteristic subregion-specific changes can be detected in the connectivity and FA values along the rostrocaudal axis of the brainstem.

As a first step, we wanted to examine the extent of overlap between the maximum connectivity and the maximum FA voxels in the masked individual PDMs. To this end, we registered the individual FA maps to standard space and then masked these FA maps with the previously generated masked individual PDMs. Then we defined the x, y, z coordinates of the maximum connectivity and the maximum FA voxels within each axial slice between z = - 10 and z = - 48, and calculated their distance in mm.

Using the masked individual PDMs and FA maps registered to standard space, the individual mean connectivity and mean FA values were calculated for each axial slice of each subregion. Then these individual values were averaged to group mean connectivity and group mean FA values characteristic to each axial slice of the subregions. We aimed at evaluating the relationship of these group mean connectivity and FA values with the rostrocaudal position (z coordinates) of the given axial slice in standard space by performing Spearman's rank correlation and Pearson's correlation with IBM SPSS Statistics for Windows, Version 22.0. (Armonk, NY: IBM Corp. Released 2013). Significance was assumed at $p < 0.05$.

Two illustrative cases of severe traumatic brain injury

	Patient 1	Patient 2
Age at the time of injury	21	32
Sex	male	male
Mechanism of injury	fall	road collision
Glasgow Coma Score at first presentation	3	3
Initial findings on CT	small hyperintensities on the cerebral convexity	intracerebral hemorrhage in the left occipital lobe (location of a former surgery of an arteriovenous malformation)
Days from injury to MRI	12 days	19 days
MRI findings	diffuse axonal injury in the left occipital and temporal lobe, in the left cerebellar hemisphere, in the splenium of the corpus callosum and in the dorsal mesencephalon	parenchymal damage due to previous surgeries and traumatic hemorrhage in the left occipital lobe, contusion of the left cerebellar hemisphere, diffuse axonal injury in the splenium of the corpus callosum
Outcome	traumatic coma for 10 days, then gradual improvement to self-care (Barthel score[a]: 90)	traumatic coma for 16 days, then persistent vegetative state until his death 5 months after the injury

[a] (Mahoney and Barthel, 1965)

Table 3: Clinical details of the two illustrative cases of severe traumatic brain injury

Two patients with severe traumatic brain injury (TBI) (for clinical data please see Table 3) underwent the same diffusion MRI protocol and MRI data processing as described above. The mean connectivity and mean FA values for each axial slice of each subregion were calculated with one modification compared to the above described protocol: in order to obtain the FA curve along the entire

pontomesencephalic region in Patient 2 as well, we used the unthresholded but masked PDMs for the calculation of the mean FA values in case of both patients.

Results

Segmentation pattern on the group level

The medial portion of the cerebral peduncles was dominantly connected to the left and right ALIC (frontopontine CDR). This CDR could be followed downwards until the mid-pons. The middle and lateral portions of the cerebral peduncles and both sides of the pontine basis dominantly connected to the left and right PLIC (motor CDR). The dorsolateral part of the mesencephalon and the border of the pontine tegmentum and basis were dominantly connected to the sensory thalamus (sensory CDR). The mesencephalic and pontine tegmentum were dominantly connected to the medial thalamus (reticular CDR) (Figures 4 and 5).

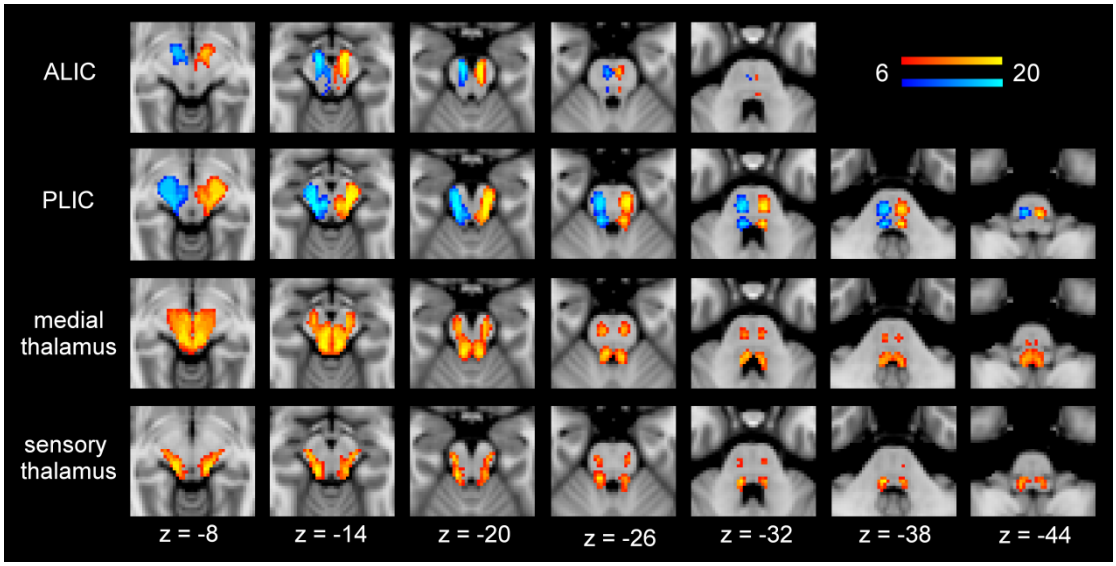

Figure 5: Intersubject variability maps overlaid on axial slices of the MNI152 2 mm brain from z = −8 to z = −44. *Maps are thresholded to contain only those voxels that showed connectivity to the corresponding target mask in at least 6 subjects. Color intensity reflects the number of subjects with a connection in the given voxel (indicated by the color bar in the upper right corner of the figure). In the first row, intersubject variability of the frontopontine probability distribution map (PDM) can be seen, showing the regions of the pontomesencephalic seed mask connecting to the target masks of the left (red-yellow) and right (blue) anterior limb of the internal capsule (ALIC). It can be seen that the frontopontine connections end in the mid-pons. In the second row, intersubject variability of the motor PDM is displayed, representing connections to the target masks of the left (red-yellow) and right (blue) posterior limb of the internal capsule (PLIC). In the third row, the intersubject variability of the reticular PDM is displayed, reflecting connectivity to the bilateral medial thalamus target mask (red-yellow). In the fourth row, intersubject variability of the sensory PDM can be seen, showing the regions that connect to the bilateral sensory thalamus target mask (red–yellow). Note that the central regions of the PDMs are highly consistent, and the overall intersubject variability is relatively low. Orientation is radiological (i.e., left = right).*

The intersubject variability maps (Figure 5) showed that the PDMs also contained collateral connections of the detected subregions. Thus, the reticular PDMs also involved areas that can be identified as the superior cerebellar peduncle, pontine nuclei and corticobulbar pathways based on their location. Furthermore, the left and right motor PDMs contained connections with sensory regions, since the target mask, the PLIC incorporates sensory pathways like the thalamocortical projections as well.

Segmentation pattern on the individual level

The individual CMs were very similar to the group CM (Figure 6) in most subjects, that is the connectivity-based segmentation of the brainstem resulted a highly consistent connectivity pattern in 13 out of the 20 healthy subjects (65%).

The distance between the individual and group CoG_{conn} locations was dominantly in the range of one voxel in MNI152 2 mm standard space (91.74% of the calculated distances were ≤ 2 mm, 7.9% were > 2 mm and ≤ 4 mm, and 0.33% were above 4 mm) reflecting good consistency of the individual results of the segmentation.

Comparison of segmentation results to microscopic anatomy and anatomical reference material

Overlaying the corresponding sections of the Nieuwenhuys atlas (Nieuwenhuys *et al.,* The human central nervous system, 3rd edition, Berlin, Springer Verlag, 1988, Figures 99 and 103, reproduced with permission) on the histological sections and the MNI152 1 mm standard brain MR images, the group CM derived by the connectivity-based segmentation of the brainstem with 25% threshold was in good overall visual concordance concerning the spatial distribution of the identified CDRs with the pathways displayed in the atlas and determined on the histological sections (Figure 6). In case of the sensory CDR, the medial lemniscus was located on the border of the motor and sensory CDRs in the mesencephalon, while in the pontine region part of it was identified in the motor CDR.

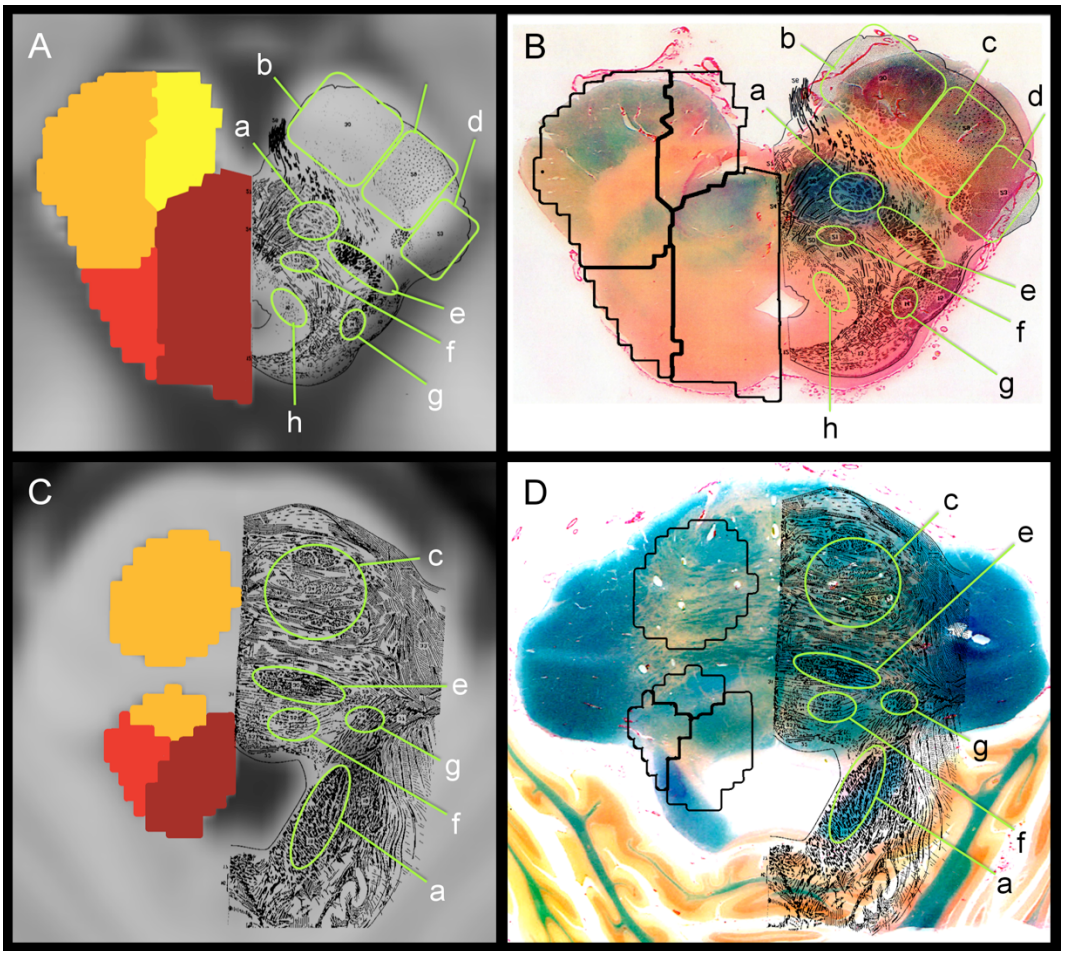

Figure 6: Comparison of the group connectivity map (CM) with histological sections and the Nieuwenhuys neuroanatomy atlas *(Nieuwenhuys et al., The human central nervous system, 3rd edition, Berlin, Springer Verlag, 1988, Figure 99 and 103. Reproduced with permission.): **A:** Level of the oculomotor nerve root: the group CM (left overlay) and the corresponding figure (Fig. 99) of the Nieuwenhuys atlas (right overlay) aligned to an axial slice of the MNI152 1 mm brain adjusted to fit the horizontal position of the histological slice on panel B. **B:** Histological section matching the level of panel A: contours of the connectivity−defined regions (CDR) of the group CM (left overlay) and corresponding figure (Fig. 99) of the Nieuwenhuys atlas (right overlay). Luxol blue – picrosirius red stain (by courtesy of the Department of Anatomy, Histology and Embryology, University of Szeged, Hungary). **C:** Level of the trigeminal nerve root: group CM (left overlay) and corresponding figure (Fig. 103) of the Nieuwenhuys atlas (right overlay) aligned to an axial slice of the MNI152 1 mm brain adjusted to fit the horizontal position of the histological slice on panel D. **D:** Histological section matching panel C: contours of the CDRs of the group CM (left overlay) and corresponding figure (Fig. 103) of the Nieuwenhuys atlas (right overlay). Luxol blue – picrosirius red stain (by courtesy of the Department of Anatomy, Histology and Embryology, University of Szeged, Hungary). Color-coding of the CMs: yellow – frontopontine CDR, orange – motor CDR, red – sensory CDR, brown – reticular CDR. Anatomical structures identified: a – superior cerebellar peduncle, b – frontopontine tract, c – corticospinal tract, d – occipitoparietotemporopontine tract, e – medial lemniscus, f – central tegmental tract, g – spinothalamic tract, h – dorsal longitudinal fasciculus. Note the good overall visual concordance of the identified CDRs with the pathways displayed in the atlas and determined on the histological sections. The medial lemniscus (e) is identified on the border of the motor and sensory CDRs on panels A and B (mesencephalon), while on panels C and D (pons), part of it can be detected within the motor CDR.*

Assessment of subregion-specific quantitative measures (connectivity, FA)

The maximum connectivity and maximum FA voxels in each axial slice of the individual PDMs overlapped in 5.5-33.5% of the cases, with the highest rate of overlap in the motor subregion and the lowest rate of overlap in the reticular subregion (Table 4). The distance between the maximum connectivity and the maximum FA voxels in each axial slice of the PDMs was ≤ 2 mm in 51.7%, > 2 mm and ≤ 4 mm in 28%, and above 4 mm in 20.3 % of the cases.

The investigation of the rostrocaudal connectivity and FA value changes in the detected subregions revealed a characteristic location-dependent pattern along the longitudinal axis of the brainstem in all subregions (Figure 7, Figure 8). The relationship of the mean connectivity values to their rostrocaudal position (represented by the z coordinate of the given axial slice) was proven to be monotonous in all subregions (all Spearman's rhos [r_S] and Pearson's coefficients [r_P] were above 0.688, $p < 0.001$). The relationship of the mean FA values to their rostrocaudal position was monotonous in the frontopontine subregion (left r_S : 0.930, left r_P : 0.921 and right r_S : 0.879, right r_P : 0.889, all $p < 0.001$), and not only monotonous but also linear in the motor subregion (left r_S : 0.997, left r_P : 0.986 and right r_S : 0.988, right r_P : 0.961, all $p < 0.001$). In the sensory (left r_S: 0.332, $p = 0.152$, left r_P: 0.430, $p = 0.058$ and right r_S: 0.320, $p = 0.169$, right r_P: 0.387, $p = 0.092$) and reticular (left r_S: 0.717, left r_P: 0.691, both $p < 0.001$ and right r_S: 0.614, right r_P: 0.620, both $p = 0.004$) subregions mean FA values were shown to be in a nearly parabolic relationship with their rostrocaudal position. That is, the highest mean FA values in the sensory and reticular subregions were observed in the upper pons, and lower values were found in the mesencephalon and the lower pons.

Subregion	Overlapping maximum connectivity and maximum FA voxels (%)	Subregion	Overlapping maximum connectivity and maximum FA voxels (%)
Left frontopontine	19.44	Left sensory	32.25
Right frontopontine	27.78	Right sensory	14.25
Left motor	33.5	Left reticular	7.5
Right motor	29.75	Right reticular	5.5

Table 4: Percentage of overlapping maximum connectivity and maximum FA voxels on the group level in the given subregion

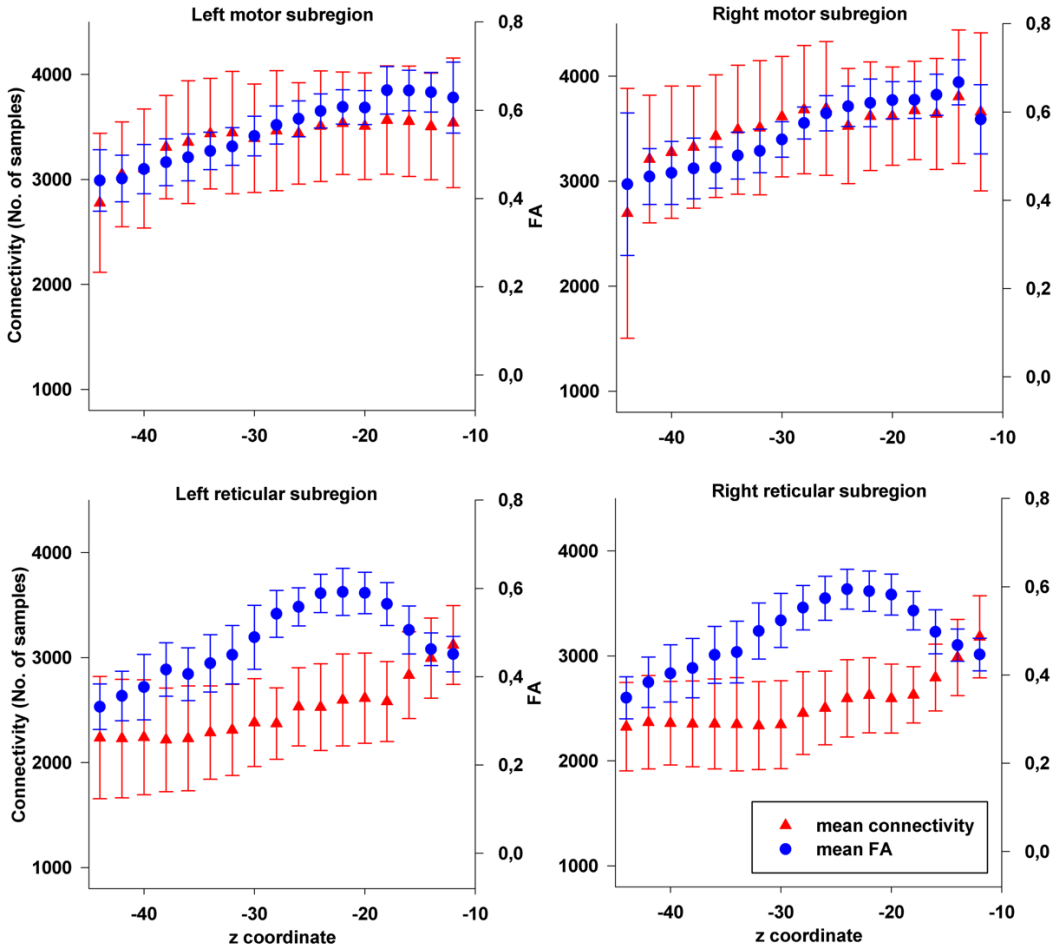

Figure 7: Plots depicting the mean connectivity and mean fractional anisotropy (FA) values in the axial slices of left and right motor and reticular subregions as a function of the z coordinate in MNI152 2 mm standard space. *Note the parallel course of the two curves in the motor subregion, in contrast to the reticular subregion, where mean connectivity values more markedly decrease in the mesencephalic region and reach a relative plateau in the pons, whereas FA values increase in the mesencephalon and start to diminish caudal to the pontomesencephalic junction.*

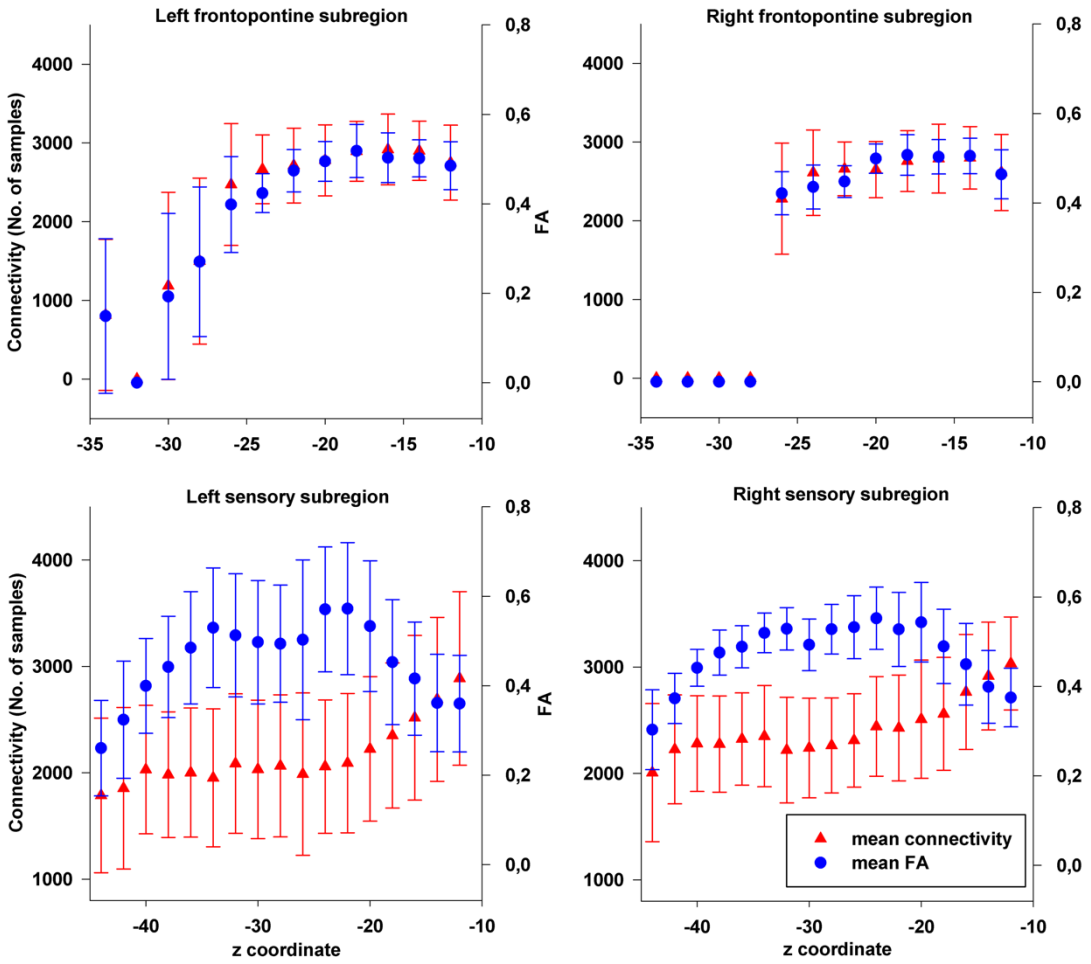

Figure 8: Plots depicting the mean connectivity and mean fractional anisotropy (FA) values in the axial slices of left and right frontopontine and sensory subregions as a function of the z coordinate in MNI152 2 mm standard space. *Note the similar mean connectivity and FA curves with monotonically decreasing values in the caudal direction in the frontopontine subregions, and the different course of the two curves in the sensory subregions, that is, the mean connectivity curve shows a monotonous decrease in the caudal direction with a relative plateau in the upper two-thirds of the pons, whereas FA values increase in the mesencephalic region, reach a plateau in the upper pons, and continue diminishing in the lower half of the pontine region.*

Two illustrative cases of severe TBI

On both the FLAIR and SWI images of Patient 1, bilateral diffuse axonal injury can be seen in the dorsal pontomesencephalic region (Figure 9), whereas in the case of Patient 2, this region appeared to be intact on these sequences. In case of Patient 1, the connectivity-based brainstem segmentation showed diminished connectivity compared with the healthy subjects in all examined subregions, but connectivity to the medial thalamus could be identified along the entire pontomesencephalic part of the brainstem that we examined. However, in the case of Patient 2, the connectivity-based brainstem segmentation revealed a more widespread damage of the brainstem with left-sided predominance. In the mesencephalon, all

subregions could be detected with diminished connectivity, but in the pontine region, connectivity was more severely decreased to the ALIC on both sides, to the left PLIC and to the left sensory thalamus (data not shown), whereas no connectivity to the medial thalamus could be identified bilaterally (Figure 10).

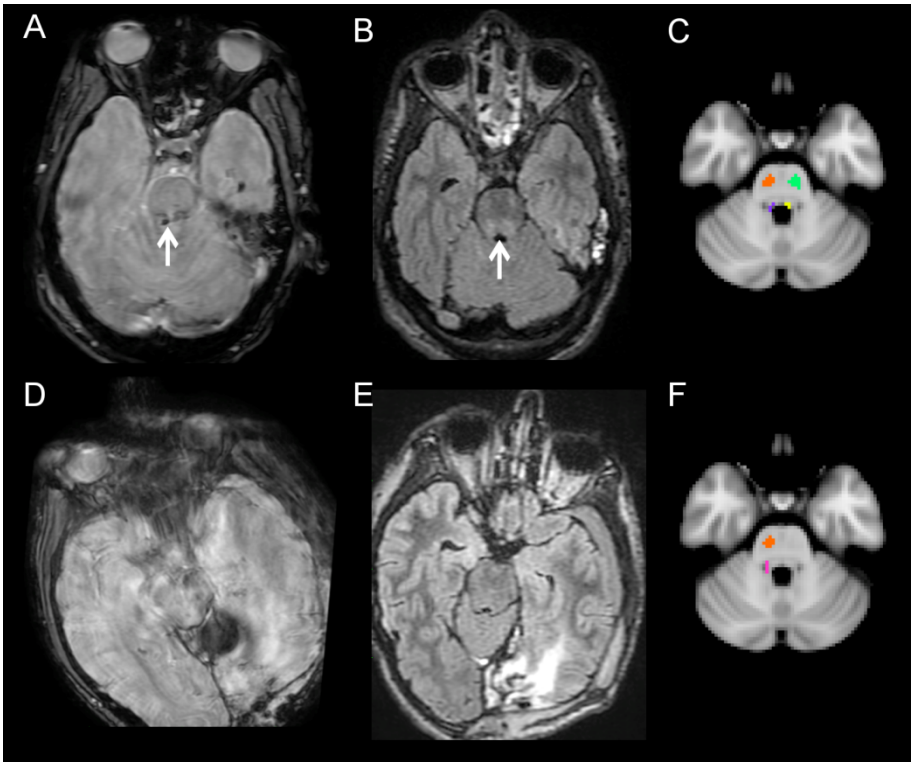

Figure 9: Potential clinical applicability of the connectivity-based brainstem segmentation in patients with severe traumatic brain injury (TBI). *In the upper row, pictures of a patient with severe TBI (Patient 1) who regained consciousness after traumatic coma can be seen, whereas in the lower row, matched pictures of a patient with severe TBI (Patient 2) who remained in a persistent vegetative state are displayed (A, D: SWI; B, E: FLAIR; C and F: results of the connectivity-based brainstem segmentation projected on the MNI152 2 mm brain. All pictures depict approximately the same level of the upper pons). In pictures A and B, signs of diffuse bilateral axonal injury can be seen in the dorsal pontomesencephalic region (white arrows), whereas in case of Patient 2, this region appears to be intact in pictures D and E. Although the results of the connectivity-based brainstem segmentation show substantial differences in both patients compared with healthy subjects, it is apparent that Patient 2 suffered a more widespread damage of the brainstem with left-sided predominance, and the reticular subregion cannot be identified as opposed to Patient 1. Color-coding: orange: right motor connectivity-defined region (CDR), green: left motor CDR, purple: right reticular CDR, yellow: left reticular CDR, pink: right sensory CDR. Orientation is radiological (i.e., left = right).*

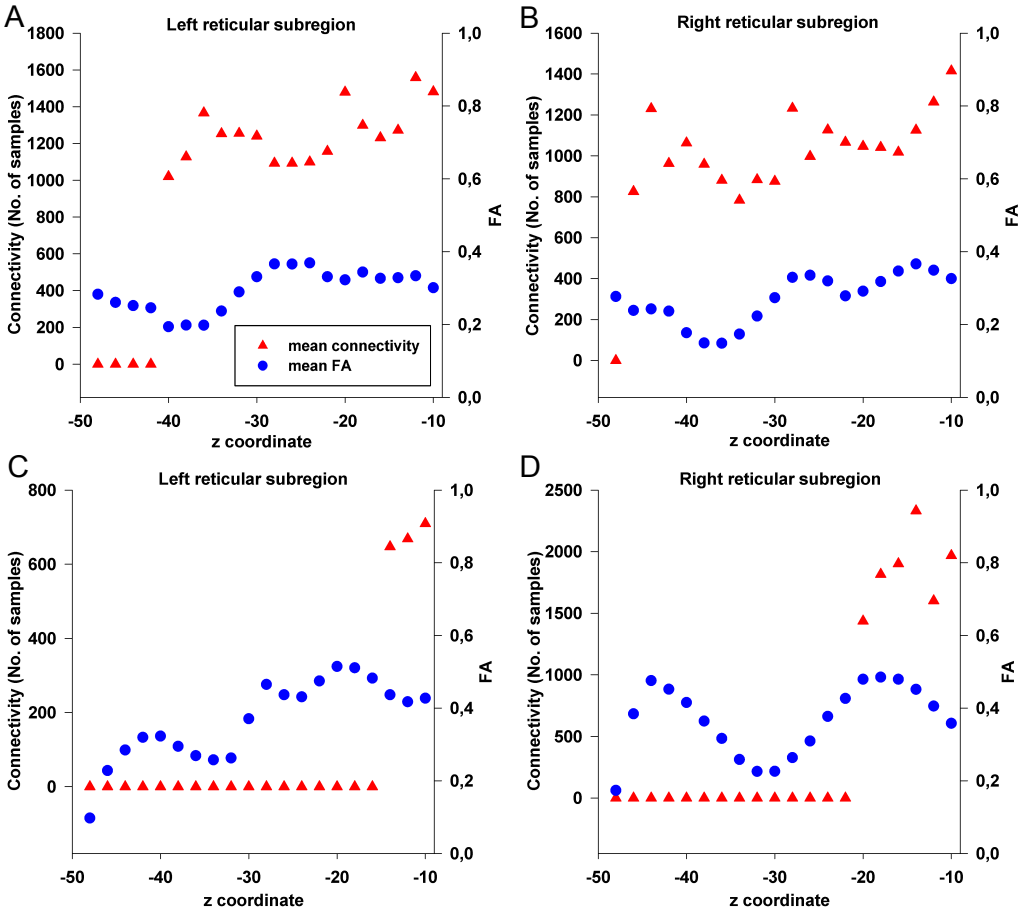

Figure 10: Plots depicting the mean connectivity and mean fractional anisotropy (FA) values in the axial slices of left and right reticular subregions as a function of the z coordinate in MNI152 2 mm standard space in two illustrative cases of severe traumatic brain injury (TBI) with different outcomes. *Plots A and B show the mean connectivity and FA curves of the reticular subregions of Patient 1, whereas plots C and D show the same curves for Patient 2. The mean connectivity curve of Patient 1 is similar to that of the healthy subjects (Fig. 7), but in case of Patient 2, no reticular connectivity can be detected along the entire pons. In Patient 1, FA values in the mesencephalon are even lower than in Patient 2, which may be the consequence of hemorrhagic lesions. However, in Patient 2, the maximum of the FA curve is also located at the pontomesencephalic junction, similarly to the healthy subjects.*

Discussion

The aim of our study was to identify quantitative measures that could be potential biomarkers in the examination of the major brainstem pathways. These biomarkers could help in the understanding and (in case of treatable pathologies) also the therapeutic decision making of several diseases such as pediatric cerebral malformations involving the pontocerebellar region, traumatic brain injury, inflammation or demyelination. As a first step we used connectivity-based segmentation by probabilistic tractography to localize four distinct brainstem subregions: 1, frontopontine; 2, motor; 3, sensory; 4, reticular formation. The

segmentation results were then verified by histological sections and a neuroanatomy atlas. Finally, we identified quantitative measures typical for these subregions. With the presentation of two severe TBI cases our aim was to demonstrate one potential clinical application of the identified biomarkers.

Correspondence of the connectivity-defined brainstem regions with the known anatomy

The location of the CDRs of the group CM showed an overall good concordance with the anatomy identified on the histological sections and a neuroanatomy atlas (Nieuwenhuys *et al.,* The human central nervous system, 3rd edition, Berlin, Springer Verlag, 1988, Figures 99 and 103, reproduced with permission), and also corresponded to the results of former DTI studies (Wakana *et al.,* 2004; Ramnani *et al.,* 2006; Habas and Cabanis, 2007; Kamali *et al.,* 2010). The good consistency of the segmentation results and the anatomy makes this method suitable for quantitative analyses of the examined brainstem subregions.

Reproducibility of the connectivity-based brainstem segmentation

The intersubject variability maps reflected a good overall consistency of the PDMs among the subjects. Each subregion was represented in the corresponding PDM in all of our subjects, with the highest connectivity values according to the expected anatomical location of the incorporated subregion. These connectivity values exhibited a decrement beyond the boundaries of the CDR detected within the given PDM (data not shown).

On the individual level, all four subregions were successfully identified by the hard segmentation in 13 out of 20 subjects (65%), but in the remaining 7 subjects the connectivity pattern of the different PDMs was similar to that of the other 13 subjects. In the 7 subjects by whom the hard segmentation failed to identify all subregions completely, the small differences between the connectivity values within the neighboring reticular and sensory PDMs could mislead the hard segmentation (as it relies on the ”winner takes it all” principle), and precluded the detection of one of these subregions.

According to our measurements, the distance between the group and individual center of gravity of the connectivity values (CoG_{conn}) was below 2 mm in 91.7 % of the cases, which shows that the CoG_{conn} of the different subjects was mostly

situated in the same or in neighboring voxels, reflecting good reproducibility of the connectivity measures within the identified subregions.

Subregion-specific quantitative measures (connectivity, fractional anisotropy)

In addition to its applicability in regions with high uncertainty, a further advantage of probabilistic tractography over deterministic methods is its suitability for quantitative measurements of connectivity. Using this advantage, our goal was to assess changes in the connectivity and fractional anisotropy (FA) values in the identified subregions along the rostrocaudal axis of the brainstem. Former studies have reported characteristic diffusion anisotropy profiles along the rostrocaudal course of the corticospinal tract (Virta *et al.,* 1999; Stieltjes *et al.,* 2001; Wakana *et al.,* 2007; Hua *et al.,* 2008) and the medial lemniscus (Stieltjes *et al.,* 2001) in the mesencephalon and the pons. A small number of studies have provided quantitative diffusion MRI values of the ascending reticular activating system (ARAS) (McNab *et al.,* 2013; Yeo *et al.,* 2013; Jang and Kwon, 2015) and the frontopontine pathways (Kamali *et al*., 2010), but as far as we know, no study has performed investigation of the rostrocaudal connectivity or FA profiles of these cerebral structures in the brainstem. Although due to the numerous differences in the applied methodology, our results are not directly comparable to the findings of these former studies, but the similar shape of the rostrocaudal FA profiles within the pontomesencephalic region observed in our study further supports the validity of our results. In case of the frontopontine subregions the mean connectivity and FA values showed a monotonous decrement in caudal direction, while in the motor subregions the curve of the mean FA values followed not only a monotonous, but a linear course. (Figures 7 and 8). As both pathways run in the cerebral peduncle, where white matter fibers have a highly ordered arrangement, this may be a possible explanation for the highest FA values observed in the mesencephalic region (Virta *et al.,* 1999). The decrease of the FA values in the caudal direction may be due to the spreading of the frontopontine fibers as they terminate on the pontine nuclei, and the interposition of the transverse pontine fibers traversing the corticospinal tract in the pons. In the reticular and sensory subregions a relative plateau of the mean connectivity values was observed in the pons, while FA profiles followed a U-shape. These characteristic changes may indicate structural differences between these subregions, and therefore may serve as potential biomarkers in the investigation of brainstem pathologies.

Skeletonizing white matter pathways according to their maximum FA voxels is a popular way to investigate microstructural white matter differences between groups of subjects (Smith *et al.,* 2006). Comparing the location of the maximum FA voxel to the maximum connectivity voxel within each axial slice of the subregions revealed that these voxels overlapped in only 5.5-33.5% of the cases, with the highest rate of overlap in the motor subregion, and the largest distances in the reticular subregion (Table 4). This finding reflects that in the majority of the cases it was not the highest FA voxel that was traversed by the highest number of samples. FA measurements are based on local diffusion parameters, while connectivity relies on more global diffusion information to characterize white matter microstructure. The high ratio of divergence between the highest FA and connectivity values raises the possibility that connectivity may be a more sensitive parameter for the investigation of the compact structure of the brainstem, especially the reticular formation. Connectivity-based segmentation of the brainstem completed with parallel investigation of the rostrocaudal changes of the connectivity and FA values may be particularly useful in the investigation of the reticular formation in disease states, considering the low FA value characteristic to this structure built up by several gray matter nuclei and interdigitating axon fibers (Purves *et al.,* 2001).

Potential clinical applicability

Our results obtained in 20 healthy subjects may provide reference for future studies investigating various pediatric and adult patient populations. The connectivity-based identification of the pontomesencephalic reticular formation may serve as a basis for quantitative studies using diffusion MRI-related biomarkers to assess the anatomical components of arousal in patients with traumatic brain injury. Former studies suggested that traumatic coma may be a result of white matter injury in the ARAS (Firsching *et al.,* 1998; Smith *et al.,* 2000), moreover, it may be the consequence of subcortical disconnection between brainstem arousal nuclei and thalamic intralaminar and reticular nuclei and the basal forebrain (Edlow *et al*., 2013). The outcome was found to be the worst in case of bilateral posterior brainstem lesions (Hilario *et al*., 2012). However, the specific pathways involved in the development of traumatic coma are still subject of intensive research (Fischer *et al.,* 2016.). In Figures 9 and 10, we present two illustrative cases of severe TBI with similar initial clinical presentation but different outcome (regained consciousness

vs. persistent vegetative state). The results of the connectivity-based brainstem segmentation would have suggested the opposite outcome for the two patients compared with the conventional MRI sequences and the FA values. These representative cases indicate that this method may provide useful additional information for the prediction of long-term outcome in patients with severe TBI. Further candidate pathologies may be space-occupying lesions (brainstem tumors), pediatric cerebral malformations affecting the pontocerebellar region, brainstem stroke (Parvizi and Damasio, 2003), and disorders of myelinisation affecting the brainstem.

Limitations

Since it is well known that diffusion MRI is sensitive to physiological noise (Bammer, 2003), various methods are available to alleviate the distortion potentially induced by cardiac and respiratory motion (e.g., cardiac gating [Habib *et al.,* 2010], or navigator-corrected approach [Alhamud *et al.,* 2015], etc.) In our study the acquisition of the DTI sequence was repeated twice and ASSET was used to increase the signal-to-noise ratio and improve image quality.

It has been shown that probabilistic tractography is inherently distance dependent (Behrens *et al.,* 2007), the more distant target points are tracked from the seed point, the lower connectivity probabilities will be resulted. As it can be observed on Figures 7 and 8, connectivity values showed a monotonous decrement in rostrocaudal direction in all examined subregions. Applying a distance correction to the connectivity values would have distorted the original connectivity measures, especially in case of group data, therefore we opted not to use distance correction in our study (Pelzer *et al.,* 2013). As there are crossing-fiber regions in the brainstem, the observed reduction of connectivity with longer distance might also reflect the effect of this phenomenon (Pelzer *et al*., 2013).

As it was highlighted by the cases of those 7 subjects, in whom not all four subregions were successfully identified, hard segmentation is insensitive of the extent of differences between connectivity values, and can be driven even by small discrepancies. Checking the PDMs can help to evaluate the connectivity in these cases.

In this study conducted with young, healthy adults we opted to use linear registration, as our aim was to keep the anatomic variability of the detected

connectivity maps (Johansen-Berg *et al.,* 2005). As all group studies face the problem of registration accuracy, the calculation of the distance between the individual CoG_{conn} locations to the group average may also be affected by registration error.

The 24-48 hours processing time can be considerably accelerated by further optimization of the sequences or increasing computational power (e.g., grid engine parallel implementation on central processing unit or graphics processing unit, improvement of the hardware resources) (Hernández *et al.,* 2013).

Applying the PLIC as a target mask instead of the primary motor cortex has advantages regarding the shorter distance between the seed and the target regions that the tracking has to cover, which may contribute to the reduction of tracking errors and may decrease the drop of connectivity values (Behrens *et al.,* 2007). Furthermore, the outlining of the PLIC mask rather than the primary motor cortex is easier, quicker and more straightforward, which speeds up preprocessing time, and the smaller number of voxels in the PLIC mask also shortens computation time. Furthermore, the uncertainty of water diffusion is considerably higher in gray matter, than in white matter, which facilitates tractography using white matter masks. A potential drawback of the PLIC in contrast to the primary motor cortex is the lower specificity of the PLIC target mask, as other pathways (e.g., occipitoparietotemporopontine and sensory fibers) are also included in the mask, and that the smaller number of voxels in the PLIC target mask may result in lower connectivity values. However, we believe that the above-mentioned advantages associated with the usage of the PLIC mask outweigh its potential lower specificity, which can be increased by segmentation of the PLIC mask, and inclusion of only those voxels that dominantly connect to motor areas.

Similarly, the sensory pathways were traced by their connectivity to the sensory thalamus defined in a standard connectivity atlas. The sensory pathways propagate adjacent to each other in the pontomesencephalic region, and our aim was to identify the region in the brainstem associated with sensory function. Despite its similar importance to the spinothalamic tract and the medial lemniscus, the trigeminal system was not highlighted in our study. However, as its main relay station in the sensory thalamus was incorporated in the sensory thalamus target mask we used, and trigeminal pathways run parallel to the other two major sensory pathways in the pontomesencephalic region (Upadhyay *et al.,* 2008), we assume that the trigeminal pathways are also represented in the detected sensory subregion.

The arbitrary selection of four simplified functional subregions for the segmentation of the brainstem can also be held a limitation of our study. Taking the complex anatomy of the brainstem into account with many smaller pathways traversing its structure, our aim was to find a reasonable compromise between clinical feasibility and specificity to elaborate a method that is still helpful in answering diagnostic and therapeutic questions. The identification of further brainstem structures by increasing the complexity and specificity of this connectivity-based brainstem segmentation can potentially be the subject of future studies.

Conclusions

In the past three decades, functional and diffusion magnetic resonance imaging have emerged from purely research methods to clinical tools, increasingly playing a role as a significant add-on in the diagnosis and therapy of CNS diseases (e.g., tumors, injuries, malformations, demyelination, etc.). During my PhD work I applied these state-of-the-art imaging techniques to develop potential non-invasive clinical tools in the diagnosis and therapy of several diseases of the CNS.

The self-paced implementation of the SYN and VIT fMRI tasks in a mixed BL/ER fashion seems to be a well-applicable alternative to a pure block-design approach, making both tasks more suitable for use in participants with both above- and below–average language abilities. Moreover, our results confirmed that the ER analysis of the paradigm provides more specific detection of the productive language network. Despite the lower design efficiency, individual sensitivity to activation was not affected. We therefore suggest that these modifications should be considered when aiming to investigate language functions in a presurgical setting in particular.

Mapping of the brainstem is challenging, which is even more true when it is affected by certain pathologies that distort the normal anatomy. Following the principles of the connectivity-based thalamus segmentation elaborated by Behrens *et al.* in 2003, we successfully segmented and identified four main functional subregions (motor, sensory, cognitive and reticular formation) in the brainstem, and found potential diffusion-tensor imaging-based quantitative biomarkers that were successfully tested in the diagnostic workup of TBI.

Both new methods warrant further research to test their applicability in various disease states and patient populations.

Acknowledgements

I would like to thank Professor Pál Barzó, my supervisor at the Department of Neurosurgery, University of Szeged for the opportunity to work in his department and for his valuable scientific guidance.

I would like to express my deep and sincere gratitude to Professor László Sztriha for his scientific advice, his continuous support of my research and pediatric neurology training activities and his sustained trust in me.

This work would not have been possible to accomplish without the assistance of my husband and colleague Dr. David Kis. I am deeply grateful for his continuous support and guidance and for that he has been always there for me either in private or professional life.

I am deeply grateful to Professor Ingeborg Krägeloh-Mann and Dr. Marko Wilke for providing me the possibility to take part of the work of the Experimental Pediatric Neuroimaging Group at the University of Tuebingen, Germany. Dr. Wilke's wide knowledge and logical way of thinking has been a great value and inspiration for me and I am also grateful for his support and care during my time in Tuebingen. I would also like to thank Dr. Karen Lidzba, Dr. Samuel Gröschel and all members of the Experimental Pediatric Neuroimaging Group for their warm welcome and outstanding collaboration.

I would like to thank Dr. László Halász and all my co-authors for their valuable help and assistance.

I would like to acknowledge Rárosi Ferenc for his technical assistance in the statistic calculations.

I would also like to thank Petra Pócza-Véger and all my colleagues at the Neurosurgery Department for all the support, entertainment and care they provided.

Finally, I am grateful to my family and friends for their support and encouragement during my work.

References

1. Abou-Khalil B, Schlaggar BL (2002) Is it time to replace the Wada test? *Neurology,* 59(2):160–161.
2. Aggarwal M, Zhang J, Pletnikova O, Crain B, Troncoso J, Mori S (2013) Feasibility of creating a high-resolution 3D diffusion tensor imaging based atlas of the human brainstem: A case study at 11.7 T. *Neuroimage* 1(74):117-127.
3. Alhamud A, Taylor PA, Laughton B, van der Kouwe AJ, Meintjes EM (2015) Motion artifact reduction in pediatric diffusion tensor imaging using fast prospective correction. *J Magn Reson Imaging* 41(5):1353-1364.
4. Andersson JL, Hutton C, Ashburner J, Turner R, Friston K (2001) Modeling geometric deformations in EPI time series. *Neuroimage* 13(5):903–919.
5. Ashburner J (2007) A fast diffeomorphic image registration algorithm. *Neuroimage* 38(1):95−113.
6. Bammer R (2003) Basic principles of diffusion-weighted imaging. *Eur J Radiol* 45(3):169-184.
7. Bandettini PA, Wong EC, Hinks RS, *et al*. (1992) Time course EPI of human brain function during task activation. *Magn Reson Med*. 25:390.
8. Basho S, Palmer ED, Rubio MA, Wulfeck B, Müller RA (2007) Effects of generation mode in fMRI adaptations of semantic fluency: Paced production and overt speech. *Neuropsychologia* 45(8):1697–1706.
9. Basser PJ, Mattiello J, LeBihan D (1994) Estimation of the effective self- diffusion tensor from the NMR spin echo. *J Magn Reson B* 103(3):247-254.
10. Basser PJ, Mattiello J, LeBihan D (1994) MR diffusion tensor spectroscopy and imaging. *Biophys J* 66(1):259-267.
11. Baxendale S, Thompson P, Duncan J, Richardson M (2003) Is it time to replace the Wada test? *Neurology* 60(2):354–355.

12. Benson RR, FitzGerald DB, LeSueur LL, Kennedy DN, Kwong KK, Buchbinder BR *et al.* (1999) Language dominance determined by whole brain functional MRI in patients with brain lesions. *Neurology* 52(4):798–809.
13. Behrens TEJ, Woolrich MW, Jenkinson M, Johansen-Berg H, Nunes RG, Clare S, Matthews PM, Brady JM, Smith SM (2003a) Characterization and propagation of uncertainty in diffusion-weighted MR imaging. *Magn Reson Med* 50(5):1077-1088.
14. Behrens TEJ, Johansen-Berg H, Jbabdi S, Rushworth MF, Woolrich MW (2007), Probabilistic diffusion tractography with multiple fibre orientations: What can we gain? *Neuroimage* 34(1):144-155.
15. Behrens TEJ, Johansen-Berg H, Woolrich MW, Smith SM, Wheeler-Kingshott CAM, Boulby PA, Barker GJ, Sillery EL, Sheehan K, Ciccarelli O, Thompson AJ, Brady JM, Matthews PM (2003b) Non-invasive mapping of connections between human thalamus and cortex using diffusion imaging. *Nat Neurosci* 6(7):750-757.
16. Binder JR, Frost JA, Hammeke TA, Bellgowan PS, Rao SM, Cox RW (1999) Conceptual processing during the conscious resting state. A functional MRI study. *J Cogn Neurosci* 11(1):80–95.
17. Binder JR, Frost JA, Hammeke TA, Cox RW, Rao SM, Prieto T (1997) Human brain language areas identified by functional magnetic resonance imaging. *J Neurosci* 17(1):353–362.
18. Binder JR, Swanson SJ, Hammeke TA, Morris GL, Mueller WM, Fischer M, *et al.* (1996) Determination of language dominance using functional MRI: A comparison with the Wada test. *Neurology* 46(4):978–984.
19. Bookheimer S (2002) Functional MRI of language: New approaches to understanding the cortical organization of semantic processing. *Annu Rev Neurosci* 25:151–188.
20. Bulheller S, Ibrahimovic N, Häcker H (2003) Entwicklung und Evaluation der deutschsprachigen Fassung des Peabody Picture Vocabulary Test (PPVT). Ein Testverfahren zur Erfassung sprachlichen Intelligenz. Frankfurt/Main: Swets Test Services.
21. Burton MW (2001) The role of inferior frontal cortex in phonological processing. *Cogn Sci* 25(5):695–709.

22. Butterworth B (1992) Disorders of phonological encoding. *Cognition* 42(1-3):261–286.
23. Chen X, Weigel D, Ganslandt O, Buchfelder M, Nimsky C (2007a) Diffusion tensor imaging and white matter tractography in patients with brainstem lesions. *Acta Neurochir* 149(11):1117-1131.
24. Chen X, Weigel D, Ganslandt O, Fahlbusch R, Buchfelder M, Nimsky C (2007b) Diffusion tensor-based fiber tracking and intraoperative neuronavigation for the resection of a brainstem cavernous angioma. *Surg Neurol* 68(3):285-291.
25. Church JA, Petersen SE, Schlaggar BL (2010) The "Task B problem" and other considerations in developmental functional neuroimaging. *Hum Brain Mapp* 31*:* 852−862.
26. Ciccarelli O, Toosy AT, Parker GJ, Wheeler-Kingshott CA, Barker GJ, Miller DH, Thompson AJ (2003) Diffusion tractography based group mapping of major white-matter pathways in the human brain. *Neuroimage* 19(4):1545-1555.
27. Clements AM, Rimrodt SL, Abel JR, Blankner JG, Mostofsky SH, Pekar JJ *et al.* (2006) Sex differences in cerebral laterality of language and visuospatial processing. *Brain Lang* 98(2):150–158.
28. Conturo TE, Lori NF, Cull TS, Akbudak E, Snyder AZ, Shimony JS *et al.* (1999) Tracking neuronal fiber pathways in the living human brain. *Proc Natl Acad Sci USA* 96(18):10422–10427.
29. Daselaar SM, Prince SE, Cabeza R (2004) When less means more: deactivations during encoding that predict subsequent memory. *Neuroimage* 23(3):921–927.
30. Demb JB, Desmond JE, Wagner AD, Vaidya CJ, Glover GH, Gabrieli JDE (1995) Semantic encoding and retrieval in the left inferior prefrontal cortex: A functional MRI study of task difficulty and process specificity. *J Neurosci* 15(9):5870–5878.
31. De Smet HJ, Paquier P, Verhoeven J, Mariën P (2013) The cerebellum: Its role in language and related cognitive and affective functions. *Brain Lang* 127(3):334–342.

32. D'Esposito M, Zarahn E, Aguirre GK, Shin RK, Auerbach P, Detre JA (1997) The effect of pacing of experimental stimuli on observed functional MRI activity. *Neuroimage* 6(2):113–121.
33. Duffau H, Moritz-Gasser S, Mandonnet E (2014) A re-examination of neural basis of language processing: Proposal of a dynamic hodotopical model from data provided by brain stimulation mapping during picture naming. *Brain Lang* 131:1–10.
34. Ebner K, Lidzba K, Hauser TK, Wilke M (2011) Assessing language and visuospatial functions with one task: A "dual use" approach to performing fMRI in children. *Neuroimage* 58(3):923–929.
35. Edlow BL, Haynes RL, Takahashi E, Klein JP, Cummings P, Benner T, Greer DM, Greenberg SM, Wu O, Kinney HC, Folkerth RD (2013) Disconnection of the ascending arousal system in traumatic coma. *J Neuropathol Exp Neurol* 72(6):505-523.
36. Edlow BL, Takahashi E, Wu O, Benner T, Dai G, Bu L, Grant PE, Greer DM, Greenberg SM, Kinney HC, Folkerth RD (2012) Neuroanatomic connectivity of the human ascending arousal system critical to consciousness and its disorders. *J Neuropathol Exp Neurol* 71(6):531-546.
37. Everts R, Lidzba K, Wilke M, Kiefer C, Mordasini M, Schroth G, *et al.* (2009) Strengthening of laterality of verbal and visuospatial functions during childhood and adolescence. *Hum Brain Mapp* 30(2):473–483.
38. Fernández G, de Greiff A, von Oertzen J, Reuber M, Lun S, Klaver P, *et al.* (2001) Language mapping in less than 15 minutes: Real-time functional MRI during routine clinical investigation. *Neuroimage* 14(3):585–594.
39. Fernández G, Specht K, Weis S, Tendolkar I, Reuber M, Fell J, *et al.* (2003) Intrasubject reproducibility of presurgical language lateralization and mapping using fMRI. *Neurology* 60(6):969–975.
40. Firsching R, Woischneck D, Diedrich M, Klein S, Rückert A, Wittig H, Döhring W (1998) Early magnetic resonance imaging of brainstem lesions after severe head injury. *J Neurosurg* 89(5):707-712.
41. Fischer DB, Boes AD, Demertzi A, Evrard HC, Laureys S, Edlow BL, Liu H, Saper CB, Pascual-Leone A, Fox MD, Geerling JC (2016) A human brain network derived from coma-causing brainstem lesions. *Neurology* 87(23):2427-2434.

42. Ford AA, Colon-Perez L, Triplett WT, Gullett JM, Mareci TH, Fitzgerald DB (2013) Imaging white matter in human brainstem. *Front Hum Neurosci* 7, Article 400. doi: 10.3389/fnhum.2013.00400.
43. Friederici AD (2002) Towards a neural basis of auditory sentence processing. *Trends Cogn Sci* 6(2):78–84.
44. Friston K (2013) Sample size and the fallacies of classical inference. *Neuroimage* 1(81):503−504.
45. Friston KJ, Holmes AP, Worsley KJ, Poline JP, Frith CD, Frackowiak RS (1995) Statistical parametric maps in functional imaging: A general linear approach. *Hum Brain Mapp* 2(4):189–210.
46. Friston KJ, Williams S, Howard R, Frackowiak RS, Turner R (1996) Movement-related effects in fMRI time-series. *Magn Res Med* 35(3):346-355.
47. Friston KJ, Worsley KJ, Frackowiak RSJ, Mazziotta JC, Evans AC (1994) Assessing the significance of focal activations using their spatial extent. *Hum Brain Mapp* 1:210−220.
48. Friston KJ, Zarahn E, Josephs O, Henson RN, Dale AM (1999) Stochastic designs in event-related fMRI. *Neuroimage* 10(5):607-619.
49. Gaillard WD, Sachs BC, Whitnah JR, Ahmad Z, Balsamo LM, Petrella JR *et al.* (2003) Developmental aspects of language processing: fMRI of verbal fluency in children and adults. *Hum Brain Mapp* 18(3):176–185.
50. Gaser C, Altaye M, Wilke M, Holland SK (2007) Unified segmentation without tissue priors. *Neuroimage* 36(Suppl. 1):S68 .
51. Genovese CR, Lazar NA, Nichols T (2002) Thresholding of statistical maps in functional neuroimaging using the false discovery rate. *Neuroimage* 15(4):870–878.
52. Giussani C, Poliakov A, Ferri RT, Plawner LL, Browd SR, Shaw DW, Filardi TZ, Hoeppner C, Geyer JR, Olson JM, Douglas JG, Villavicencio EH, Ellenbogen RG, Ojemann JG (2010) DTI fiber tracking to differentiate demyelinating diseases from diffuse brain stem glioma. *Neuroimage* 52(1):217-223.
53. Golay X, Jiang H, van Zijl PC, Mori S (2002) High-resolution isotropic 3D diffusion tensor imaging of the human brain. *Magn Reson Med* 47(5):837-843.
54. Grodd W, Hülsmann E, Ackermann H (2005) Functional MRI localizing in the cerebellum. *Neurosurg Clin N Am 16*(1):77–99.

55. Habas C, Cabanis EA (2007) Anatomical parcellation of the brainstem and cerebellar white matter: A preliminary probabilistic tractography study at 3 T. *Neuroradiology* 49(10):849-863.
56. Habib J, Auer DP, Morgan PS (2010) A quantitative analysis of the benefits of cardiac gating in practical diffusion tensor imaging of the brain. *Magn Reson Med* 63(4):1098-1103.
57. Hagoort P (2005) On Broca, brain, and binding: A new framework. *Trends Cogn Sci 9*(9):416–423.
58. Helton KJ, Phillips NS, Khan RB, Boop FA, Sanford RA, Zou P, Li CS, Langston JW, Ogg RJ (2006) Diffusion tensor imaging of tract involvement in children with pontine tumors. *AJNR Am J Neuroradiol* 27(4):786-793.
59. Helton KJ, Weeks JK, Phillips NS, Zou P, Kun LE, Khan RB, Gajjar A, Fouladi M, Broniscer A, Boop F, Li CS, Ogg RJ (2008) Diffusion tensor imaging of brainstem tumors: axonal degeneration of motor and sensory tracts. *J Neurosurg Pediatr* 1(4):270-276.
60. Hernández M, Guerrero GD, Cecilia JM, García JM, Inuggi A, Jbabdi S, Behrens TE, Sotiropoulos SN (2013) Accelerating fibre orientation estimation from diffusion weighted magnetic resonance imaging using GPUs. *PLoS One* 8(4):e61892. doi: 10.1371/journal.pone.0061892.
61. Hilario A, Ramos A, Millan JM, Salvador E, Gomez PA, Cicuendez M, Diez-Lobato R, Lagares A (2012) Severe traumatic head injury: prognostic value of brainstem injuries detected by MRI. *AJNR Am J Neuroradiol* 33(10):1925-1931.
62. Hinojosa JA, Martín-Loeches M, Gómez-Jarabo G, Rubia FJ (2000) Common basal extrastriate areas for the semantic processing of words and pictures. *Clin Neurophysiol* 111(3):552–560.
63. Hodaie M, Quan J, Chen DQ (2010) In vivo visualization of cranial nerve pathways in humans using diffusion-based tractography. *Neurosurgery* 66(4):788-795.
64. Hong JH, Son SM, Jang SH (2010) Somatotopic location of corticospinal tract at pons in human brain: A diffusion tensor tractography study. *Neuroimage* 51(3):952-955.
65. Hua K, Zhang J, Wakana S, Jiang H, Li X, Reich DS, Calabresi PA, Pekar JJ, van Zijl PC, Mori S (2008) Tract probability maps in stereotaxic spaces:

Analyses of white matter anatomy and tract-specific quantification. *Neuroimage* 39(1):336-347.

66. Jang SH, Kwon HG (2015) The ascending reticular activating system from pontine reticular formation to the hypothalamus in the human brain: A diffusion tensor imaging study. *Neurosci Lett* 17(590):58-61.
67. Jansen A, Flöel A, Van Randenborgh J, Konrad C, Rotte M, Förster AF *et al.* (2005) Crossed cerebro-cerebellar language dominance. *Hum Brain Mapp* 24(3):165–172.
68. Jenkinson M, Bannister P, Brady M, Smith S (2002) Improved optimization for the robust and accurate linear registration and motion correction of brain images. *Neuroimage* 17(2):825-841.
69. Jenkinson M, Beckmann CF, Behrens TEJ, Woolrich M W, Smith SM (2012) FSL. *Neuroimage* 62(2):782-790.
70. Jenkinson M, Smith SM (2001) A global optimisation method for robust affine registration of brain images. *Med Image Anal* 5(2):143-156.
71. Johansen-Berg H, Behrens TEJ, Sillery E, Ciccarelli O, Thompson AJ, Smith SM, Matthews PM (2005) Functional-anatomical validation and individual variation of diffusion tractography-based segmentation of the human thalamus. *Cereb Cortex* 15(1):31-39.
72. Jones DK (2008) Studying connections in the living human brain with diffusion MRI. *Cortex* 44(8):936-952.
73. Kamali A, Kramer LA, Butler IJ, Hasan KM (2009) Diffusion tensor tractography of the somatosensory system in the human brainstem: Initial findings using high isotropic spatial resolution at 3.0 T. *Eur Radiol* 19(6):1480-1488.
74. Kamali A, Kramer LA, Frye RE, Butler IJ, Hasan KM (2010) Diffusion tensor tractography of the human brain cortico-ponto-cerebellar pathways: A quantitative preliminary study. *J Magn Reson Imaging* 32(4):809-817.
75. Karnath HO, Rüter J, Mandler A, Himmelbach M (2009) The anatomy of object recognition−visual form agnosia caused by medial occipitotemporal stroke. *J Neurosci* 29(18):5854–5862.
76. Khorrami MS, Faro SH, Seshadri A, Moonat S, Lidicker J, Hershey BL *et al*. (2011) Functional MRI of sensory motor cortex: comparison between finger-to-thumb and hand squeeze tasks. *J Neuroimaging* 21(3):236-240.

77. Kis D, Máté A, Kincses ZT, Vörös E, Barzó P (2014) The role of probabilistic tractography in the surgical treatment of thalamic gliomas. *Neurosurgery* 10(Suppl 2):262-272.
78. Kotsoni E, Byrd D, Casey BJ (2006) Special considerations for functional magnetic resonance imaging of pediatric populations. *J Magn Reson Imaging,* 23(6), 877–886.
79. Kovanlikaya I, Firat Z, Kovanlikaya A, Uluğ AM, Cihangiroglu MM, John M, Bingol CA, Ture U (2011) Assessment of the corticospinal tract alterations before and after resection of brainstem lesions using Diffusion Tensor Imaging (DTI) and tractography at 3T. *Eur J Radiol* 77(3):383-391.
80. Krienen FM, Buckner RL (2009) Segregated fronto-cerebellar circuits revealed by intrinsic functional connectivity. *Cereb Cortex* 19(10):2485-2497.
81. Krinzinger H, Koten JW, Hennemann J, Schueppen A, Sahr K, Arndt D *et al.* (2011) Sensitivity, reproducibility, and reliability of self-paced versus fixed stimulus presentation in an fMRI study on exact, non-symbolic arithmetic in typically developing children aged between 6 and 12 years. *Dev Neuropsychol* 36(6):721–740.
82. Kwong KK, Belliveau JW, Chesler DA *et al.* (1992) Dynamic magnetic resonance imaging of human brain activity during primary sensory stimulation. *Proc Natl Acad Sci USA* 89:5675.
83. Lazar M (2010) Mapping brain anatomical connectivity using white matter tractography. *NMR Biomed* 23(7): 821–835.
84. LeBihan D, Mangin JF, Poupon C *et al*. (2001) Diffusion tensor imaging: concepts and applications. *J Magn Reson Imaging* 13(4):534-546.
85. Lehericy S, Cohen L, Bazin B, Samson S, Giacomini E, Rougetet R *et al.* (2000) Functional MR evaluation of temporal and frontal language dominance compared with the Wada test. *Neurology* 54:1625–1633.
86. Leiner HC, Leiner AL, Dow RS (1989) Reappraising the cerebellum: What does the hindbrain contribute to the forebrain? *Behav Neurosci* 103(5):998–1008.
87. Leiner HC, Leiner AL, Dow RS (1991) The human cerebro-cerebellar system: its computing, cognitive, and language skills. *Behav Brain Res* 44(2):113-128.
88. Levelt WJ (1992) Accessing words in speech production: Stages, processes and representations. *Cognition* 42(1-3):1-22.

89. Lidzba K, Schwilling E, Grodd W, Krägeloh-Mann I, Wilke M (2011) Language comprehension vs. language production: Age effects on fMRI activation. *Brain Lang* 119(1):6–15.
90. Lidzba K, Wilke M, Staudt M, Krägeloh-Mann I, Grodd W (2008) Reorganization of the cerebro-cerebellar network of language production in patients with congenital left-hemispheric brain lesions. *Brain Lang* 106(3):204–210.
91. Liu TT (2012) The development of event-related fMRI designs. *Neuroimage* 62(2):1157-1162.
92. Lui YW, Law M, Chacko-Mathew J, Babb JS, Tuvia K, Allen JC, Zagzag D, Johnson G (2007) Brainstem corticospinal tract diffusion tensor imaging in patients with primary posterior fossa neoplasms stratified by tumor type: A study of association with motor weakness and outcome. *Neurosurgery* 61(6):1199-1207.
93. Macey PM, Macey KE, Kumar R, Harper RM (2004) A method for removal of global effects from fMRI time series. *Neuroimage* 22(1):360–366.
94. Mahoney FI, Barthel D (1965) Functional evaluation: The Barthel Index. *Md State Med J* 14:56-61.
95. McNab JA, Edlow BL, Witzel T, Huang SY, Bhat H, Heberlein K, Feiweier T, Liu K, Keil B, Cohen-Adad J, Tisdall MD, Folkerth RD, Kinney HC, Wald LL (2013) The Human Connectome Project and beyond: initial applications of 300 mT/m gradients. *Neuroimage* 15(80):234-245.
96. Mechelli A, Henson RN, Price CJ, Friston KJ (2003) Comparing event-related and epoch analysis in blocked design fMRI. *Neuroimage* 18(3):806-810.
97. Mechelli A, Price CJ, Henson RN, Friston KJ (2003) Estimating efficiency a priori: A comparison of blocked and randomized designs. *Neuroimage* 18(3):798-805.
98. Meola A, Yeh FC, Fellows-Mayle W, Weed J, Fernandez-Miranda JC (2016) Human Connectome-Based Tractographic Atlas of the Brainstem Connections and Surgical Approaches. *Neurosurgery* 79(3):437-455.
99. Mori S, Crain BJ, Chacko VP, Van Zijl PC (1999) Three dimensional tracking of axonal projections in the brain by magnetic resonance imaging. *Ann Neurol* 45(2): 265-269.

100. Mori S, Kaufmann WE, Davatzikos C, *et al*. (2002) Imaging cortical association tracts in the human brain using diffusion-tensor-based axonal tracking. *Magn Reson Med* 47(2):215-223.

101. Nagae-Poetscher LM, Jiang H, Wakana S, Golay X, van Zijl PC, Mori S (2004) High-resolution diffusion tensor imaging of the brain stem at 3 T. *AJNR Am J Neuroradiol* 25(8):1325-1330.

102. Newton JM, Ward NS, Parker GJ, Deichmann R, Alexander DC, Friston KJ, Frackowiak RS (2006) Non-invasive mapping of corticofugal fibres from multiple motor areas - relevance to stroke recovery. *Brain* 129(7):1844-1858.

103. Nieuwenhuys R, Voogd J, van Huijzen C (1988) The human central nervous system, 3rd edition. pp 110-111&118-119. Berlin: Springer Verlag.

104. Ogawa S, Lee TM (1990) Magnetic resonance imaging of blood vessels at high fields: in vivo and in vitro measurements and image simulation. *Magn Reson Med* 16(1):9-18.

105. Ogawa S, Lee TM, Kay AR, *et al.* (1990) Brain magnetic resonance imaging with contrast dependent on blood oxygenation. *Proc Natl Acad Sci USA* 87(24):9868-9872.

106. Ogawa S, Lee TM, Nayak AS, Glynn P (1990) Oxygenation-sensitive contrast in magnetic resonance image of rodent brain at high magnetic fields. *Magn Reson Med* 14(1):68-78.

107. Ogawa S, Menon RS, Tank DW, *et al.* (1993) Functional brain mapping by blood oxygenation level-dependent contrast magnetic resonance imaging. A comparison of signal characteristics with a biophysical model. *Biophys J* 64(3):803-812.

108. Oldfield RC (1971) The assessment and analysis of handedness: The Edinburgh inventory. *Neuropsychologia* 9(1):97-113.

109. Pagani E, Filippi M, Rocca MA, Horsfield MA (2005) A method for obtaining tract-specific diffusion tensor MRI measurements in the presence of disease: Application to patients with clinically isolated syndromes suggestive of multiple sclerosis. *Neuroimage* 26(1):258-265.

110. Parvizi J, Damasio AR (2003) Neuroanatomical correlates of brainstem coma. *Brain* 126(Pt 7):1524-1536.

111. Pelzer EA, Hintzen A, Goldau M, von Cramon DY, Timmermann L, Tittgemeyer M (2013) Cerebellar networks with basal ganglia: Feasibility for

tracking cerebello-pallidal and subthalamo-cerebellar projections in the human brain. *Eur J Neurosci* 38(8):3106-3114.

112. Petersen SE, Dubis JW (2012) The mixed block/event-related design. *Neuroimage* 62(2):1177-1184.
113. Phillips NS, Sanford RA, Helton KJ, Boop FA, Zou P, Tekautz T, Gajjar A, Ogg RJ (2005) Diffusion tensor imaging of intraaxial tumors at the cervicomedullary and pontomedullary junctions. Report of two cases. *J Neurosurg* 103(6 Suppl):557-562.
114. Pillai JJ, Allison JD, Sethuraman S, Araque JM, Thiruvaiyaru D, Ison CB *et al.* (2004) Functional MR imaging study of language-related differences in bilingual cerebellar activation. *AJNR Am J Neuroradiol* 25(4):523-532.
115. Poldrack RA, Paré-Blagoev EJ, Grant PE (2002) Pediatric functional magnetic resonance imaging: Progress and challenges. *Top Magn Reson Imaging* 13(1):61-70.
116. Prabhu SP, Ng S, Vajapeyam S, Kieran MW, Pollack IF, Geyer R, Haas-Kogan D, Boyett JM, Kun L, Poussaint TY (2011) DTI assessment of the brainstem white matter tracts in pediatric BSG before and after therapy: A report from the Pediatric Brain Tumor Consortium. *Childs Nerv Syst* 27(1):11-18.
117. Price C (2000) The anatomy of language: Contributions from functional neuroimaging. *J Anat* 197:335-359.
118. Price CJ, Veltman DJ, Ashburner J, Josephs O, Friston KJ (1999) The critical relationship between the timing of stimulus presentation and data acquisition in blocked designs with fMRI. *Neuroimage* 10(1):36-44.
119. Purves D, Augustine GJ, Fitzpatrick D, Katz LC, LaMantia A-S, O McNamara J, Williams SM (2001) Motor control centers in the brainstem: Upper motor neurons that maintain balance and posture. In: *Neuroscience.* 2nd edition. Sunderland (MA): Sinauer Associates. http://www.ncbi.nlm.nih.gov/books/NBK11081/
120. Ramnani N, Behrens TEJ, Johansen-Berg H, Richter MC, Pinsk MA, Andersson JL, Rudebeck P, Ciccarelli O, Richter W, Thompson AJ, Gross CG, Robson MD, Kastner S, Matthews PM (2006) The evolution of prefrontal inputs to the cortico-pontine system: Diffusion imaging evidence from Macaque monkeys and humans. *Cereb Cortex* 16(6):811-818.

121. Riecker A, Ackermann H, Wildgruber D, Dogil G, Grodd W (2000) Opposite hemispheric lateralization effects during speaking and singing at motor cortex, insula and cerebellum. *Neuroreport* 11:1997–2000.

122. Rorden C, Karnath HO, Bonilha L (2007) Improving lesion-symptom mapping. *J Cogn Neurosci* 19(7):1081-1088.

123. Ruff IM, Petrovich Brennan NM, Peck KK, Hou BL, Tabar V, Brennan CW *et al.* (2008) Assessment of the language laterality index in patients with brain tumor using functional MR imaging: Effects of thresholding, task selection, and prior surgery. *AJNR Am J Neuroradiol* 29(3):528–535.

124. Salamon N, Sicotte N, Alger J, Shattuck D, Perlman S, Sinha U, Schultze-Haakh H, Salamon G (2005) Analysis of the brain-stem white-matter tracts with diffusion tensor imaging. *Neuroradiology* 47(12):895-902.

125. Seurinck R, Vingerhoets G, Vandemaele P, Deblaere K, Achten E (2005) Trial pacing in mental rotation tasks. *Neuroimage* 25(4):1187–1196.

126. Smith DH, Nonaka M, Miller R, Leoni M, Chen XH, Alsop D, Meaney DF (2000) Immediate coma following inertial brain injury dependent on axonal damage in the brainstem. *J Neurosurg* 93(2):315-322.

127. Smith SM (2002) Fast robust automated brain extraction. *Hum Brain Mapp* 17(3):143-155.

128. Smith SM, Jenkinson M, Johansen-Berg H, Rueckert D, Nichols TE, Mackay CE, Watkins KE, Ciccarelli O, Cader MZ, Matthews PM, Behrens TEJ (2006) Tract-based spatial statistics: Voxelwise analysis of multi-subject diffusion data. *Neuroimage* 31(4):1487-1505.

129. Smith SM, Jenkinson M, Woolrich MW, Beckmann CF, Behrens TEJ, Johansen-Berg H, Bannister PR, De Luca M, Drobnjak I, Flitney DE, Niazy RK, Saunders J, Vickers J, Zhang Y, De Stefano N, Brady JM, Matthews PM (2004) Advances in functional and structural MR image analysis and implementation as FSL. *Neuroimage* 23(S1):208-219.

130. Soria G, De Notaris M, Tudela R, Blasco G, Puig J, Planas AM, Pedraza S, Prats-Galino A (2011) Improved assessment of ex vivo brainstem neuroanatomy with high-resolution MRI and DTI at 7 Tesla. *Anat Rec* 294(6):1035-1044.

131. Stejskal EO, Tanner JE (1965) Spin diffusion measurements: spin echoes in the presence of a time-dependent field gradient. *J Chem Phys* 42(1):288-292.

132. Stieltjes B, Kaufmann WE, van Zijl PC, Fredericksen K, Pearlson GD, Solaiyappan M, Mori S (2001) Diffusion tensor imaging and axonal tracking in the human brainstem. *Neuroimage* 14(3):723-735.

133. Szaflarski JP, Binder JR, Possing ET, McKiernan KA, Ward BD, Hammeke TA (2002) Language lateralization in left-handed and ambidextrous people: fMRI data. *Neurology* 59(2):238–244.

134. Szaflarski JP, Holland SK, Schmithorst VJ, Byars AW (2006) fMRI study of language lateralization in children and adults. *Hum Brain Mapp* 27(3):202–212.

135. Thirion B, Pinel P, Mériaux S, Roche A, Dehaene S, Poline JB (2007) Analysis of a large fMRI cohort: Statistical and methodological issues for group analyses. *Neuroimage* 35(1):105–120.

136. Thulborn KR, Waterton JC, Matthews PM, Radda GK (1982) Oxygenation dependence of the transverse relaxation time of water protons in whole blood at high field. *Biochim Biophys Acta* 714(2):265-270.

137. Tieleman A, Seurinck R, Deblaere K, Vandemaele P, Vingerhoets G, Achten E (2005) Stimulus pacing affects the activation of the medial temporal lobe during a semantic classification task: An fMRI study. *Neuroimage* 26(2):565–572.

138. Ulrich NH, Kockro RA, Bellut D, Amaxopoulou C, Bozinov O, Burkhardt JK, Sarnthein J, Kollias SS, Bertalanffy H (2014) Brainstem cavernoma surgery with the support of pre- and postoperative diffusion tensor imaging: Initial experiences and clinical course of 23 patients. *Neurosurg Rev* 37(3):481-491.

139. Upadhyay J, Knudsen J, Anderson J, Becerra L, Borsook D (2008) Noninvasive mapping of human trigeminal brainstem pathways. *Magn Reson Med* 60(5):1037-1046.

140. van Ermingen-Marbach M, Grande M, Pape-Neumann J, Sass K, Heim S (2013) Distinct neural signatures of cognitive subtypes of dyslexia with and without phonological deficits. *Neuroimage Clin* 2:477–490.

141. Virta A, Barnett A, Pierpaoli C (1999) Visualizing and characterizing white matter fiber structure and architecture in the human pyramidal tract using diffusion tensor MRI. *Magn Reson Imaging* 17(8):1121-1133.

142. Wakana S, Caprihan A, Panzenboeck MM, Fallon JH, Perry M, Gollub RL, Hua K, Zhang J, Jiang H, Dubey P, Blitz A, van Zijl P, Mori S (2007)

Reproducibility of quantitative tractography methods applied to cerebral white matter. *Neuroimage* 36(3):630-644.

143. Wakana S, Jiang H, Nagae-Poetscher LM, van Zijl PC, Mori S (2004) Fiber tract-based atlas of human white matter anatomy. *Radiology* 230(1):77-87.
144. Wilke M (2012) An alternative approach towards assessing and accounting for individual motion in fMRI timeseries. *Neuroimage* 59(3):2062–2072.
145. Wilke M, Holland SK (2008) Structural MR imaging studies of the brain in children: Issues and opportunities. *Neuroembryology and Aging* 5:6–13.
146. Wilke M, Lidzba K (2007) LI-tool: A new toolbox to assess lateralization in functional MR−data. *J Neurosci Methods* 163(1):128–136.
147. Wilke M, Lidzba K, Staudt M, Buchenau K, Grodd W, Krägeloh-Mann I (2005) Comprehensive language mapping in children, using functional magnetic resonance imaging: What's missing counts. *Neuroreport* 16(9):915–919.
148. Wilke M, Lidzba K, Staudt M, Buchenau K, Grodd W, Krägeloh-Mann I (2006) An fMRI task battery for assessing hemispheric language dominance in children. *Neuroimage* 32(1):400–410.
149. Wilke M, Pieper T, Lindner K, Dushe T, Holthausen H, Krägeloh-Mann I (2010) Why one task is not enough: Functional MRI for atypical language organization in two children. *Eur J Paediatr Neurol* 14(6):474–478.
150. Wilke M, Pieper T, Lindner K, Dushe T, Staudt M, Grodd W *et al.* (2011) Clinical functional MRI of the language domain in children with epilepsy. *Hum Brain Mapp* 32(11):1882–1893.
151. Wilke M, Schmithorst VJ (2006) A combined bootstrap/histogram analysis approach for computing a lateralization index from neuroimaging data. *Neuroimage* 33(2):522–530.
152. Wilke M, Schmithorst VJ, Holland SK (2002) Assessment of spatial normalization of whole-brain magnetic resonance images in children. *Hum Brain Mapp* 17:48–60.
153. Witwer B, Moftakhar R, Hasan K *et al.* (2002) Diffusion-tensor imaging of white matter tracts in patients with cerebral neoplasm. *J Neurosurg* 97(3):568-575.

154. Woolrich MW, Jbabdi S, Patenaude B, Chappell M, Makni S, Behrens TEJ, Beckmann C, Jenkinson M, Smith SM (2009) Bayesian analysis of neuroimaging data in FSL. *Neuroimage* 45(1 Suppl):S173-186.

155. World Medical Association - Declaration of Helsinki – Ethical principles for medical research involving human subjects. (2013) *JAMA* 310(20):2191–2194. doi:10.1001/jama.2013.281053

156. Yeo SS, Chang PH, Jang SH (2013) The ascending reticular activating system from pontine reticular formation to the thalamus in the human brain. *Front Hum Neurosci* 7: Article 416. doi: 10.3389/fnhum.2013.00416.

157. Yerys BE, Jankowski KF, Shook D, Rosenberger LR, Barnes KA, Berl MM *et al.* (2009) The fMRI success rate of children and adolescents: Typical development, epilepsy, attention deficit/hyperactivity disorder, and autism spectrum disorders. *Hum Brain Mapp* 30(10):3426–3435.

158. Yuan W, Altaye M, Ret J, Schmithorst V, Byars AW, Plante E *et al.* (2009) Quantification of head motion in children during various fMRI language tasks. *Hum Brain Mapp* 30(5):1481–1489.

159. Zsoter A, Staudt M, Wilke M (2012) Identification of successful clinical fMRI sessions in children: An objective approach. *Neuropediatrics* 43(5):249–257.